Research article

JGS
Journal of the Geological Society

https://doi.org/10.1144/jgs2025-144 | Vol. 183 | 2026 | jgs2025-144

Giant injectite complex sand body architecture in the Late Jurassic East Greenland rift

Steven D. Andrews[1]*, Ed Keavney[1], David M. Hodgson[1], Jeff Peakall[1], Ian A. Kane[2], Bonita J. Barrett[3], Ian Sharp[3] and Mark A. Scott[3]

[1] School of Earth and Environment, University of Leeds, Leeds, UK
[2] Department of Earth and Environmental Sciences, University of Manchester, Manchester, UK
[3] Equinor ASA, Bergen, Norway
SDA, 0000-0002-0418-0809; DMH, 0000-0003-3711-635X; JP, 0000-0003-3382-4578; IAK, 0000-0002-0371-4223; BJB, 0000-0002-3274-822X; IS, 0000-0002-2999-7698
* Correspondence: steven.andrews914@gmail.com

Abstract: The geometries of kilometre-scale sandstone injectite complexes, and the models developed for their emplacement, are based on a scarce dataset of large sandstone intrusion complexes. The Hareelv Formation of the Jameson Land Basin (East Greenland) provides one of the best outcrop examples of a large-scale (>4000 km^2) injectite complex within an extensional tectonic setting. We used 3D photogrammetric models and field observations to characterize the large-scale geometries of the Hareelv Formation injectite sand bodies and propose a new model for closed system injectite complexes. The Hareelv Formation sand bodies are up to 50 m thick and 1–2 km wide. Common features include steps, low-angle discordant wings, host rock rafts, bifurcations, linking complexes and stockworks. No physical evidence for linkage to the palaeoseabed, nor candidate parent units, is present. The Hareelv Formation injectites are therefore inferred to have acted as a closed system: self-sourced and dominated by lateral injection. The distribution of the sealing organic-rich, laminated host mudstones exerts a primary control on the development of injectites in the Jameson Land Basin and adjacent regions. The self-sourced lateral intrusion processes may provide a more appropriate mechanism for the interpretation of subsurface examples where the identification of source units is uncertain.

Received 8 July 2025; **revised** 10 November 2025; **accepted** 11 November 2025

Sandstone injectites are an important component of many deep-marine sedimentary successions (Jolly and Lonergan 2002; Hurst *et al.* 2003, 2011; Huuse *et al.* 2005). However, the existing models for large-scale (kilometre-scale) injectites are largely based on the exceptionally exposed Panoche Giant Injection Complex (PGIC) in the deep-water Paleogene strata of the San Joaquin Basin (Vigorito *et al.* 2008; Vétel and Cartwright 2010) and lower resolution geophysical datasets (e.g. Huuse *et al.* 2007). Reliance on examples from a limited range of tectonic settings and/or subsurface data, with the inherent limitations in resolution, risks overlooking the potential for greater variety in the geometries and formation mechanisms of these intriguing systems.

The long recognized, but difficult to access, Late Jurassic injectite complex of Jameson Land (East Greenland; Figs 1, 2) has the potential to broaden our understanding of large-scale injectite complexes, forming one of very few global examples to be well exposed over such a large aerial extent. The Hareelv Formation, which hosts the intrusive complexes, currently crops out and sub-crops over an area of *c.* 4000 km^2 (Fig. 1). The Hareelv Formation injectite complex lies within the range of large sandstone intrusion complexes (LSICs) defined by Cartwright (2010), which includes the North Sea Basin (40 000 km^2), the Faroe–Shetland Basin (2000 km^2) and the San Joaquin Basin, including the PGIC (300–400 km^2 exposed extent).

Our aim is to provide the first large-scale characterization of the sandstone injection complexes hosted within the Hareelv Formation of the Jameson Land Basin. This is made possible through the use of uncrewed aerial vehicles to build georeferenced 3D photogrammetric models. Alongside large-scale 3D models, tied to detailed field observations, comparison with subsurface datasets was possible through the examination of onshore borehole data collected by the Geological Survey of Greenland in the 1980s and 1990s and by the Geological Survey of Denmark and Greenland in 2008 (Bjerager *et al.* 2018) (Fig. 1).

Our specific objectives were: (1) to provide a broader view of the large-scale sand body architectures that provides a greater context for the more detailed work of previous studies (Surlyk 1987; Surlyk and Noe-Nygaard 2001, 2003; Surlyk *et al.* 2007); (2) to refine the depositional interpretation and model for remobilization; and (3) to use the best known exhumed example of an LSIC in an extensional setting to reduce uncertainties in predicting the distribution and character (connectivity, geometries, and the nature and extent of intraformational baffles, barriers and mudstone rafts) of buried injectite complexes in similar tectonic settings on the UK and Norwegian continental shelves.

Geological background

The Jameson Land Basin lies between 70° and 73° N on the East Greenland coast (Figs 1, 2). Rifting along the East Greenland margin commenced in the Devonian following the collapse of the Caledonian Orogen (McClay *et al.* 1986; Surlyk 1990) and continued in phases through the Carboniferous, Permian and Triassic (Surlyk 1990; Seidler *et al.* 2004; Andrews *et al.* 2021). Renewed major rifting across East Greenland, which would ultimately lead to the opening of the North Atlantic Ocean, initiated in the Mid- to Late Jurassic (Surlyk 1990). North of Jameson Land, tilted fault blocks developed at this time (Parsons *et al.* 2017; Surlyk *et al.* 2021). However, the subsidence in Jameson Land appears to have been controlled by a single north–south-oriented fault that bounded the western margin of the basin, with Jurassic strata onlapping the eastern margin (Fig. 1). Bjerager *et al.* (2018)

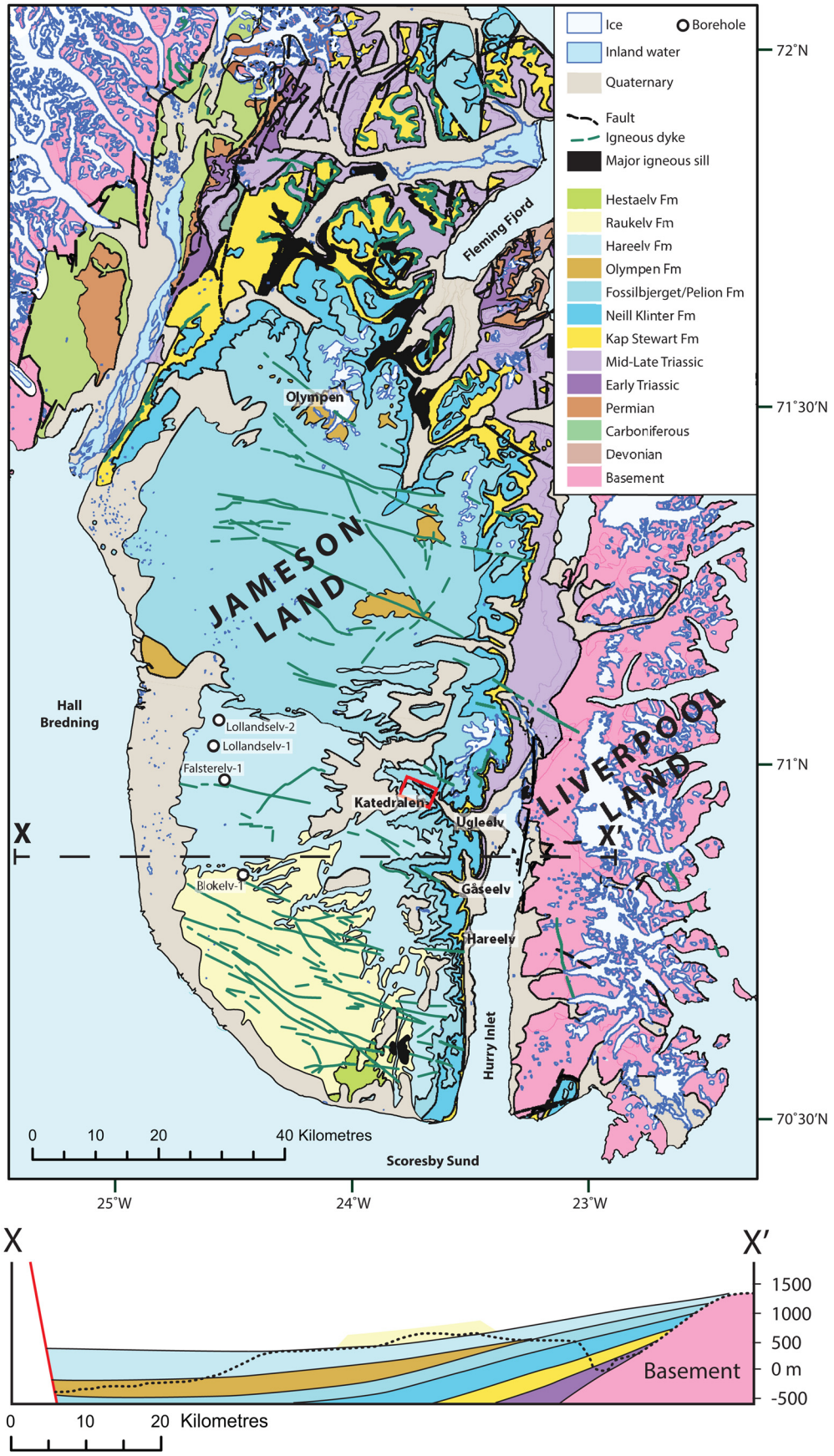

Fig. 1. Geological map of Jameson Land and Liverpool Land, with the key localities labelled, and cross-section with strata projected beyond the present-day erosion surface (dotted black line). The position of the cross-section is marked by the dashed line (X–X′) on the geological map. The wider regional setting is provided in Figure 2. Source: geological map modified after Henriksen (1984) and cross-section modified after Bjerager *et al.* (2018).

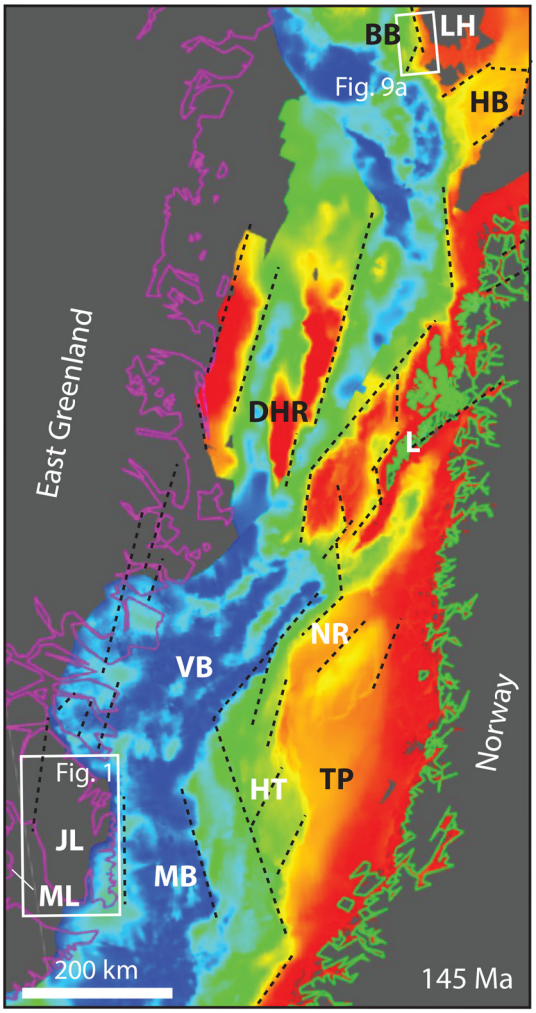

Fig. 2. Reconstruction of the North Atlantic for the latest Jurassic created using G-Plates (Equinor internal production, Müller *et al.* 2018; using Matthews *et al.* 2016) with the major faults marked as dashed black lines and the position of Figure 1 and Figure 9a indicated by white boxes. The coloured base map is a regional base Cretaceous two-way travel time composite seismic surface. MB, Møre Basin; VB, Vøring Basin; HT, Halten Terrace; TP, Trondelag Platform; NR, Nordland Ridge; L, Loføten; HB, Hammerfest Basin; LH, Loppa High; BB, Bjørnøya Basin; DHR, Dennmarks Haven Ridge; JL, Jameson Land; ML, Milne Land.

illustrated a westwards-thickening in the Hareelv Formation from *c.* 240 to 360 m.

The Mid- to Late Jurassic was a time of rising sea-levels, resulting in a transition from early Jurassic shallow marine and estuarine deposition (the Neill Klinter Group) to back-stepping shallow marine (the Pelion Formation) and ultimately deep-water deposition (the Hareelv Formation) during the Late Jurassic (Fig. 3). Seen within a regional North Atlantic context, the onlapping and over-stepping transgressive paralic to shelfal succession of the Middle Jurassic sediments of East Greenland are assigned to the rift initiation phase of Jurassic rifting, whereas the overlying deepening succession of deep-marine mudstones and associated gravity-flow sandstones of the Late Jurassic are assigned to the rift climax phase, which culminated in accelerated faulting phases in the Kimmeridgian and Volgian (Underhill and Partington 1993; Surlyk 2003). Rifting accelerated through the Early Cretaceous to the north of the Jameson Land Basin, as rifting stepped progressively eastwards, resulting in the deposition of a thick succession of deep-water mudstones (Surlyk 1990; Parsons *et al.* 2017). In Jameson Land, the latest Jurassic–Early Cretaceous comprises the *c.* 400 m thick shelfal clastic sediments of the

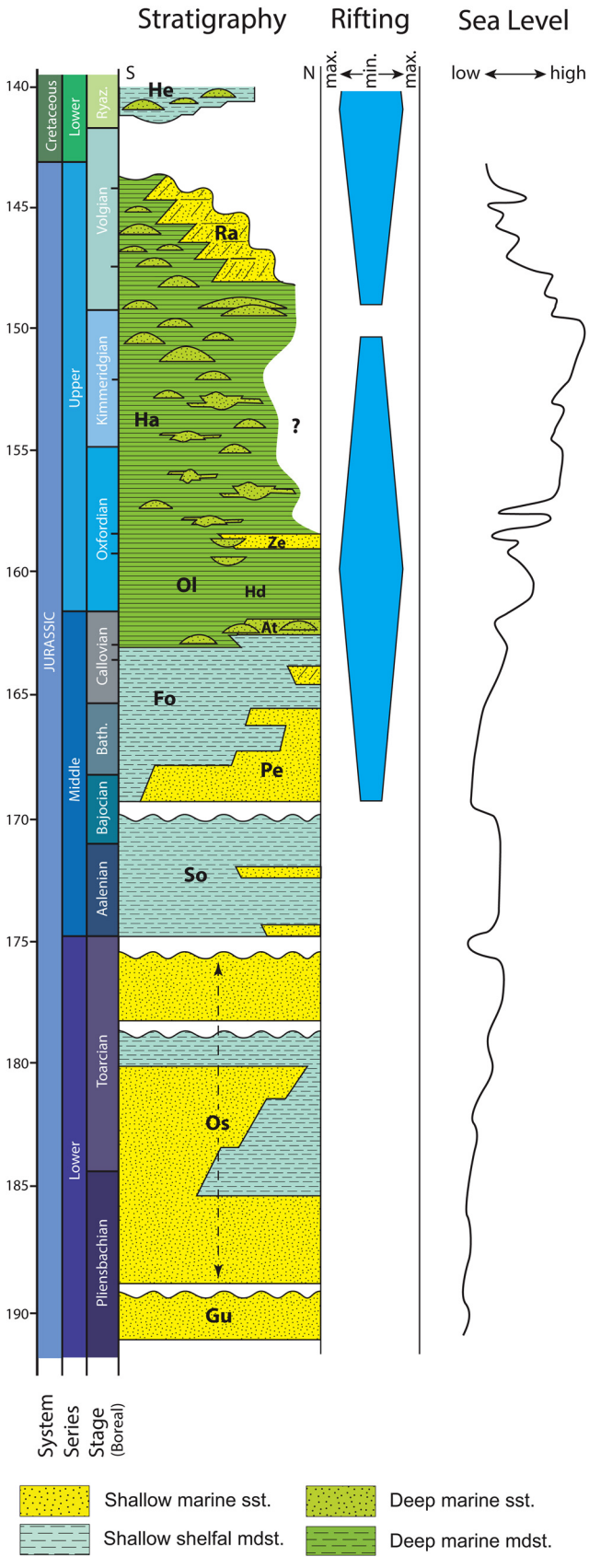

Fig. 3. Late Jurassic stratigraphy of the Jameson Land Basin. Gu, Gule Horn Formation; Os, Ostreaelv Formation; So, Sortehat Formation; Pe, Pelion Formation; Fo, Fossilbjerget Formation; Ol, Olympen Formation (At, Athene Member; Hd, Hades Member; Ze, Zeus Member); Ha, Hareelv Formation; Ra, Raukelv Formation; He, Hesteelv Formation; Bath., Bathonian; Ryaz., Ryazanian. Source: Jurassic timescale from Hesselbo *et al.* (2020); sea-level curves compiled from Surlyk (1990) and Bjerager *et al.* (2018).

Raukelv Formation that prograded from the western basin margin during the Volgian (Surlyk *et al.* 2021; Surlyk and Larsen 2023). The Early Cretaceous shelf margin canyon-fill of the Hesteelv Formation (120 m: Surlyk *et al.* 2021) forms the youngest preserved deposits in the basin.

The deposition of the Hareelv Formation took place from the mid-Oxfordian to the lower Volgian (Surlyk *et al.* 2021) and the sandstone bodies it contains have been interpreted as representing slope gully-fills and gully mouth/lobe deposits in a deep-marine setting (Surlyk 1987). Palaeocurrent indicators provide evidence for sediment input from both the NE and the NW (Surlyk 1987). Exposures of more proximal equivalents to these systems are limited by the present-day erosion levels in the north of Jameson Land; however, Bruhn and Surlyk (2004) documented a Callovian to middle Oxfordian shelfal to deep-water succession in central Jameson Land. Analogous younger systems may have fed sand-rich systems in the Hareelv Formation, but the limitations of exposure have resulted in palaeogeographical reconstructions that lack detail for this period (Surlyk 2003).

Previous work on the Hareelv Formation sand bodies

Remobilized and intruded sandstone bodies were first reported from the Late Jurassic of Jameson Land by Surlyk *et al.* (1973). Surlyk (1987) provided the first detailed description of the Hareelv Formation sand bodies, interpreting deposition in steep-sided gullies, up to 50 m thick, and laterally extensive gully mouth/lobe deposits, several hundred metres wide, which displayed no architectural organization. Primary sedimentary structures, aside from weak stratification, were notable for their absence from the sand bodies. The absence of sedimentary structures, alongside the apparently overhanging nature of some gully walls, loading and the presence of sandstone sills (metres thick) and dykes (up to 0.3 m wide) was attributed to the widespread liquefaction of the sandstone bodies following their rapid deposition from high-density flows. Dykes and sills were identified by their sharp discordant boundaries and abrupt lateral changes in thickness.

Based on their observations of the ptygmatic folding of dykes, Surlyk (1987) calculated a post-injection compaction percentage of 30–50% for the host mudstones and used this to interpret that injection occurred at burial depths of 0–60 m (Surlyk 1987). The gully wall and gully axis orientations support sediment input from the NE, linked to shallow marine systems similar to those described from the Olympen Formation (Larsen and Surlyk 2003; Bruhn and Surlyk 2004), and from the NW, attributed to systems analogous to those exhumed on Milne Land, which stretched along the western basin margin. A model was presented where the sand bodies represented point-sourced gully-fills and associated lobes, where each gully and lobe recorded a single event and did not receive multiple flows (Surlyk 1987).

Surlyk and Noe-Nygaard (2001, 2003) expanded this work to focus on the remobilization of the sand within the Hareelv Formation, presenting a model where slope gullies were developed through retrogressive slumping, then filled by successive sandy debris flows/liquefied flows, with loading occurring into the gully margins and the formation of consolidation lamination and dish structures. Fluidization was interpreted to have occurred during shallow burial, generating the mounding of sand body tops and the injection of dykes and sills. The earlier dykes were considered to have been subjected to ptygmatic folding during deeper burial (tens of metres), at which time a further cross-cutting set of intrusions formed with a more rectilinear arrangement, following incipient fracture/joint networks. Sand remobilization was interpreted to result largely from cyclic seismic loading (Surlyk and Noe-Nygaard 2001, 2003).

Surlyk *et al.* (2007) revisited the Hareelv Formation injectite model. Here, the gully features are depicted as wide (*c.* 4 km) and, although still noted to form through retrogressive slumping, it was suggested that they underwent periods of sediment by-pass before subsequent infill. Initial remobilization occurred during shallow burial, with loading into the surrounding mudstones forming over-steepened margins. During deeper burial, joints and fractures formed and were utilized by sills and dykes that were injected from the main sand bodies.

Several issues remain around the proposed models. For example, the absence of evidence of remobilization within the mudstone units, including the lack of any slide, slump or debris flow deposits; the ability of the mudstones to slump, to leave steep gully margins, and yet be loaded into and compacted by 30–50%; the lack of any erosive products within the sandstones; the difficulty in building multiple generations of overpressure at relatively shallow depths; and the lack of extrudite development from injection occurring at very shallow levels (tens of metres). Crucially, if some of the remobilization features did develop during deposition or in shallow burial, then it is difficult to explain why similar features are not observed in time-equivalent successions containing sand bodies that have been identified as similar to those that might have existed prior to the remobilization of those in the Hareelv Formation (e.g. the Athene Member of the Olympen Formation; Surlyk 1987).

Methods

A 3D georeferenced photogrammetric model was built of the cliffs on the southern side of Ugleelv that extend westwards for *c.* 5 km from Katedralen (Fig. 4). Photo sets were collected using a DJI Phantom 4 uncrewed aerial vehicle and the model was constructed using Agisoft (2022). Interpretations were made in Virtual Reality Geological Studio (VRGeoscience Limited, 2022; Hodgetts *et al.* 2015). Sand body geometries were constructed from interpreted panels captured from VRGS. The region was traversed by foot, but not all of the exposures were examined in detail in the field. Where possible, palaeocurrent indicators were measured. Orientations of planar surfaces, such as sand body margins, were measured in VRGS with calculated orientations taken from the plane defined by the intersection of the sand body margin and the model topography.

Sand body geometries

Twelve discrete sand bodies were identified in the *c.* 5 km long east–west cliff section (Fig. 4a) that defines the southern side of Ugleelv. The strata appear flat-lying, with the regional dip measuring <3° to the SW. Although the individual cliff sections provide 2D outcrops, the indented nature of the entire cliff section allows a broader appreciation of the 3D geometry of the features recognized. The identified sand bodies are differentiated from one another based on vertical and lateral separation, with each sand body consisting of a thicker core region and laterally tapering margins. The basal contacts are commonly concordant with the host rock in the central portion of each sand body and tend to become discordant towards their lateral extremities (Fig. 4). The sand bodies are up to 50 m thick and extend laterally up to 1330 m, and potentially up to 2000 m (composite extent of sand body 9; Fig. 4). The sand bodies consist of fine- to medium-grained sandstone and contain little observable internal structure. The host laminated mudstones are dark grey to black, organic-rich and appear unbioturbated. The sand bodies are described from west (sand body 1) to east (sand body 12, Fig. 4a).

Sand body 1

Sand body 1 can be traced for 1330 m across the cliffs of Katedralen and reaches a composite thickness of 50 m (Fig. 4b). The thicker

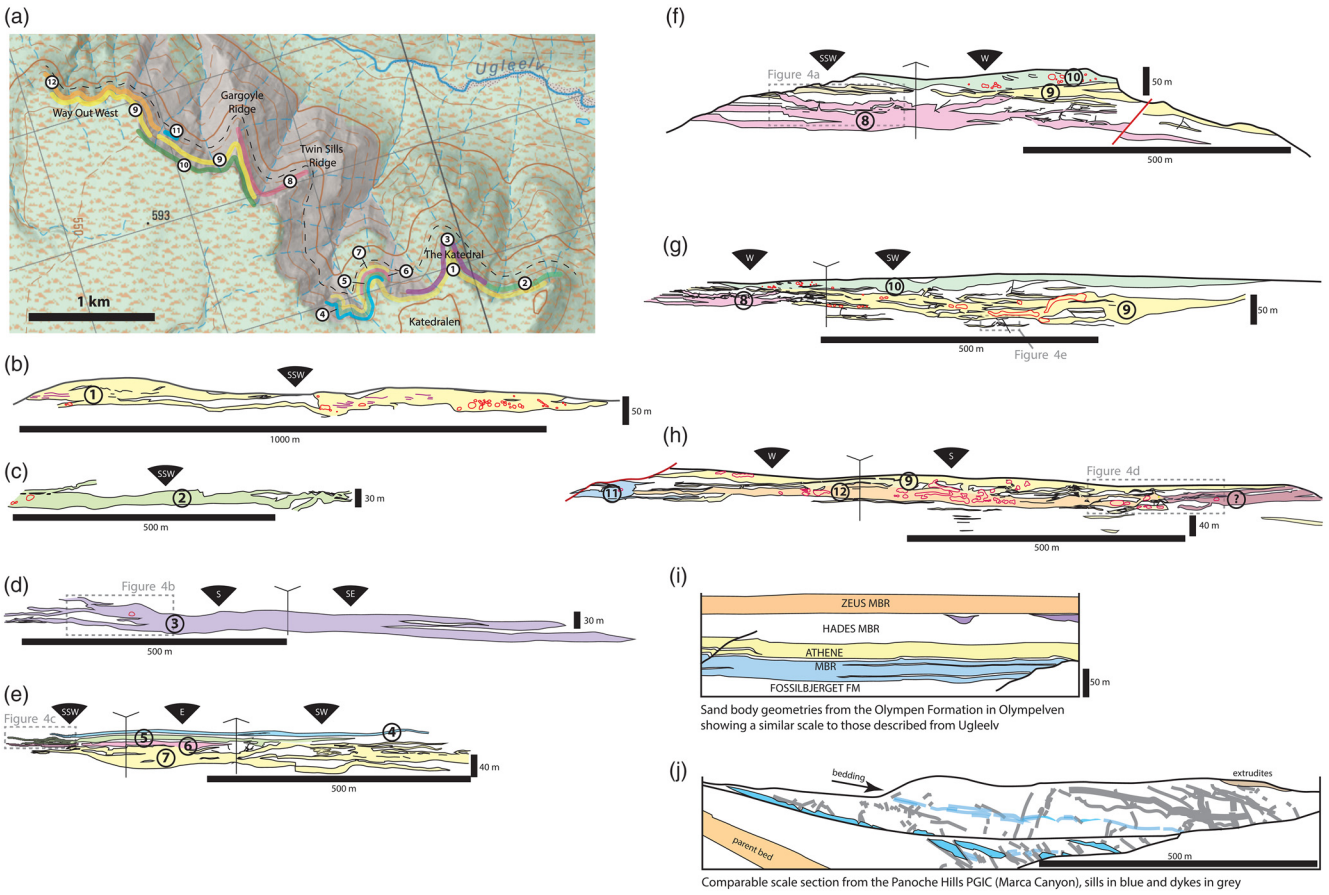

Fig. 4. Sand body geometries within the Hareelv Formation. (**a**) Relative positions of the illustrated sand bodies in the cliffs of Ugleelv and the base of the Hareelv Formation (black dashed line). (**b**–**h**) Line traces of the 12 discrete sand bodies identified in the southern cliffs of Ugleelv (Hareelv Formation) and comparison with (**i**) sand bodies in the up-system Olympen Formation and (**j**) a similar scale of outcrop segment from the Panoche Giant Injection Complex. Contours are at 50 m spacing and the location of the map is provided in Figure 1. Note: due to the relief of the cliff sections, the exact scale does vary across the panels. The purple lines indicate the orientation of banding, the red polygons denote large-scale concretions and the cross-cutting red lines indicate faults. Source: part (a) basemap licence (CC BY 4.0) Danish Climate Data Agency (https://dataforsyningen.dk/data); part (j) after Vigorito *et al.* (2008).

upper portion has steep-sided contacts (up to 35°) with the host mudstones. A laterally extensive sill (11 m thick) links the lower portions of this sand body across the exposure, pinching out to the SW and linking to the underlying sand body 2 to the east. The upper contact of the sand body is uneven. Large sub-horizontal rafts of the host mudstones (up to 50 m long by 2 m thick) displaying mild deformation define distinct horizons in the upper portion of this sand body. Smaller rafts are also present, but are often more widely distributed.

Internally, 10–50 mm thick banding is recognized. The banding is largely sub-horizontal, even adjacent to the steeper sand body margins, with locally developed lateral convergence and divergence (Fig. 4b, purple lines). Large-scale spherical (up to 10 m diameter), sphero-cylindrical (3 × 17 m) and dumb-bell (4.5 × 20 m with 6 m diameter 'bells') concretions are present, concentrated towards the base of the sand body where it reaches its thickest extent.

Sand body 2

Sand body 2 extends for 650 m across the eastern extremity of the Katedralen cliffs and terminates at a valley to the east (Fig. 4c). This sand body is broadly sub-horizontal, reaches a maximum thickness of 30 m in the east, and thins and bifurcates westwards. At its thickest, a contiguous band of mudstone rafts aligns with the split-off point of a sill that steepens, cutting up stratigraphy obliquely and linking with the overlying sand (sand body 1). To the west, sand body 2 varies in thickness, with abrupt thinning occurring where the upper surface steps downwards. A complex array of off-shooting sills (0.01–4 m thick) and linking dykes occurs at its eastern extremity, where it connects to the thickest portion of sand body 1. A set of thin (<4 m thick) sills links laterally to sand body 3.

No internal structure was observed in this sand body. However, much of the exposure is poorly consolidated and therefore this would likely obscure any available detail. Large-scale (up to 9 m diameter) spherical concretions are recorded where this sand body is thickest.

Sand body 3

Sand body 3 is exposed around the northern spur of Katedralen, where it extends across 650 m and reaches a maximum thickness of 30 m (Fig. 4d). Towards the SSE, the sand body passes obliquely upwards (40 m) and bifurcates into several thin (<6 m) horizontal/sub-horizontal sills. In places, bifurcated fingers rejoin, forming an anastomosing network and separating slabs (2.5 m thick) of the host mudstone. The most complex expression is developed beneath one of the thickest portions of sand body 1, where linkages upwards to both it, and laterally to sand body 2, occur. To the SW, sand body 3 splits into two leaves, the upper of which contains an extensive raft of the host mudstone (*c.* 150 m wide). No internal structure was observed within this sand body and few concretions were noted.

Sand body 4

Sand body 4 forms the topmost of three bodies with relatively simple geometries that overlie the more extensive sand body 7

(Fig. 4e). These sand bodies lie on the cliffs between Katedralen and Twin Sill Ridge. Reaching a maximum thickness of 12 m, sand body 4 can be traced for 730 m, thinning at both ends. To the east, sand body 4 passes upwards obliquely and then links to sand body 1; to the west, poor exposure obscures its ultimate termination. Towards its centre, at its thickest point, a 60 m long raft of the host mudstone is noted.

Sand body 5

Sand body 5 reaches a maximum thickness of 12 m and extends laterally for 770 m (Fig. 4e). At its eastern extremity it bifurcates, with most of the bifurcating branches stepping upwards, although local down-stepping is also noted. Where the bifurcating branches approach the underlying sand body 6, arrays of thin (0.1–0.2 m) low- and high-angle dykes are developed, linking the larger sand bodies. At its western termination, it links into sand body 7 before thinning and pinching out. In this region, dykes up to 9 m thick that link to 2.5 m thick sills are also noted. The apparent thickness of these dykes may be a product of the angle of outcrop intersection because the longer (23 m) dykes that link to sand body 7 in the same area are <0.1 m thick.

Sand body 6

At 400 m wide, sand body 6 is one of the least laterally extensive units recorded (Fig. 4e). It reaches a maximum thickness of 9 m and steps up and tapers towards its margins. In some instances, the steps are mirrored in underlying sand body 7. The top of sand body 6 is uneven and links to sand body 5 through low-angle injections. A sharp break between two aligned sand body segments is also noted in the east. To the west, the base of the sand body becomes amalgamated with the underlying sand body 7.

Sand body 7

Sand body 7 is complex and can be traced for >750 m before the exposure becomes poor in the west (Fig. 4e). A maximum thickness of 40 m is reached in its eastern half. The presence of mudstone rafts, up to 40 m long, which are distributed along discrete horizons, suggest that this thickness results from the amalgamation of multiple sand bodies. Laterally, these raft horizons align with more laterally extensive mudstone units that separate the sandstone bodies.

Towards the eastern margin, the base of sand body 7 passes upwards obliquely and the total thickness becomes separated by mudstone intercalations, although low-angle linkages between the individual sand units are still noted. The top of sand body 7 is uneven and, in some instances, displays steps that follow those in the overlying sand body. To the west, sand body 7 bifurcates into three sub-horizontal units that amalgamate and split once more at the western extremity of the exposed section, where several of the sills thin and pinch out. Where amalgamation occurs, aligned rafts of mudstone up to 50 m long are noted. Commonly, these rafts transition laterally into more continuous inter-sand-body mudstone units. The mudstone rafts have tapered terminations and display a consistent thickness, but often have uneven tops and bases. More chaotic sand body geometries, often consisting of linked sub-horizontal elements, are also associated with areas of amalgamation.

Sand body 8

Sand body 8 extends laterally for >650 m and reaches a maximum thickness of 45 m in its central portion, where several aligned rafts, up to 55 m long, define undulatory horizons (Fig. 4f). The raft horizons align with laterally continuous mudstone units to the east, where sand body 8 splits into three sills, each up to 15 m thick. These sills step up and thin to the east and appear to cross-cut thinner sub-horizontal sand bodies, which themselves taper to the east. The uppermost sill appears to consist of several linked rotated blocks (Fig. 5a). To the west, sand body 8 bifurcates, with the individual elements commonly passing upwards obliquely and thinning (1–3 m). Well-exposed vertically linking dykes also become common. Examples of wavy to convolute lamination are recorded in some portions of the sandstone body; rare thin beds (0.05 m thick) containing current ripple cross-lamination are also observed in this unit.

Sand body 9

Sand body 9 can be traced for 900 m, possibly extending for a further 1000 m to the west (Fig. 4g). It has a maximum thickness of 42 m towards its western margin, where it displays an uneven basal contact, cutting down up to 20 m. The top of sand body 9 in this area is undulose, exhibiting a relief of up to 10 m. To the east, rafts of mudstone (>100 m long, 6 m thick) delineate discrete horizons. The larger rafts contain sandstone lenses and arrays of low- and high-angle dykes. Several discrete sills that pass upwards obliquely are recognized towards the eastern termination of sand body 9. These tend to amalgamate and split eastwards. This pattern might be related to the proximity of sand bodies 8 and 10, which both link to sand body 9. Thinner sills (1–2 m thick and up to 150 m long), with common bifurcation, tend to be distributed above and below the main sand body. These sills are often linked to the main sand body via decimetre thick vertical to subvertical dykes. In some instances, these thinner sills contain breaks (15 m) that are filled by a stockwork of centimetre- to decimetre-scale sandstone veins.

In some areas, where the sandstones are well cemented, discontinuous *c.* 0.1 m banding is observed. Large-scale nodules are present throughout sand body 9, but do show some preferential distribution towards the base of the unit. Spherical (5 m diameter), rarer sphero-cylindrical (up to 22 m long) and more irregular forms (90 m long and often resembling linked spheroidal forms) are all recognized.

Sand body 10

Sand body 10 defines the top of the cliff section where it is exposed and therefore the character of its upper contact is not clear (Fig. 4g). It extends laterally over 1100 m, although the eastern limit is poorly exposed, and reaches a maximum thickness of 37 m. Its basal contact is uneven, displaying relief of up to 13 m, and tends to cut upwards obliquely towards the sand body margins. In the east, the base of this unit is amalgamated with sand body 9, with the contact delineated by several mudstone rafts. Overall, mudstone rafts are relatively rare within sand body 10, although a few aligned clusters are recorded in the east, where they define an undulating horizon. High- and low-angle dykes provide linkages to sand body 9 in the central areas of the exposure. Spherical (up to 10 m diameter) and sphero-cylindrical nodules are present, largely found towards the base of the thickest portion of sand body 10.

Sand body 11

Sand body 11 is somewhat irregular in form, with a lower portion (120 × 30 m) consisting of two linked bulbous elements connected to an upper tabular portion (130 m long), linked by a 35 m wide vertical conduit (Fig. 4h). A link to sand body 12 occurs to the west. The eastern margin is offset by a fault that has been exploited by an igneous dyke. Rare spherical nodules, up to 5 m in diameter, are noted, but have no obvious pattern of distribution.

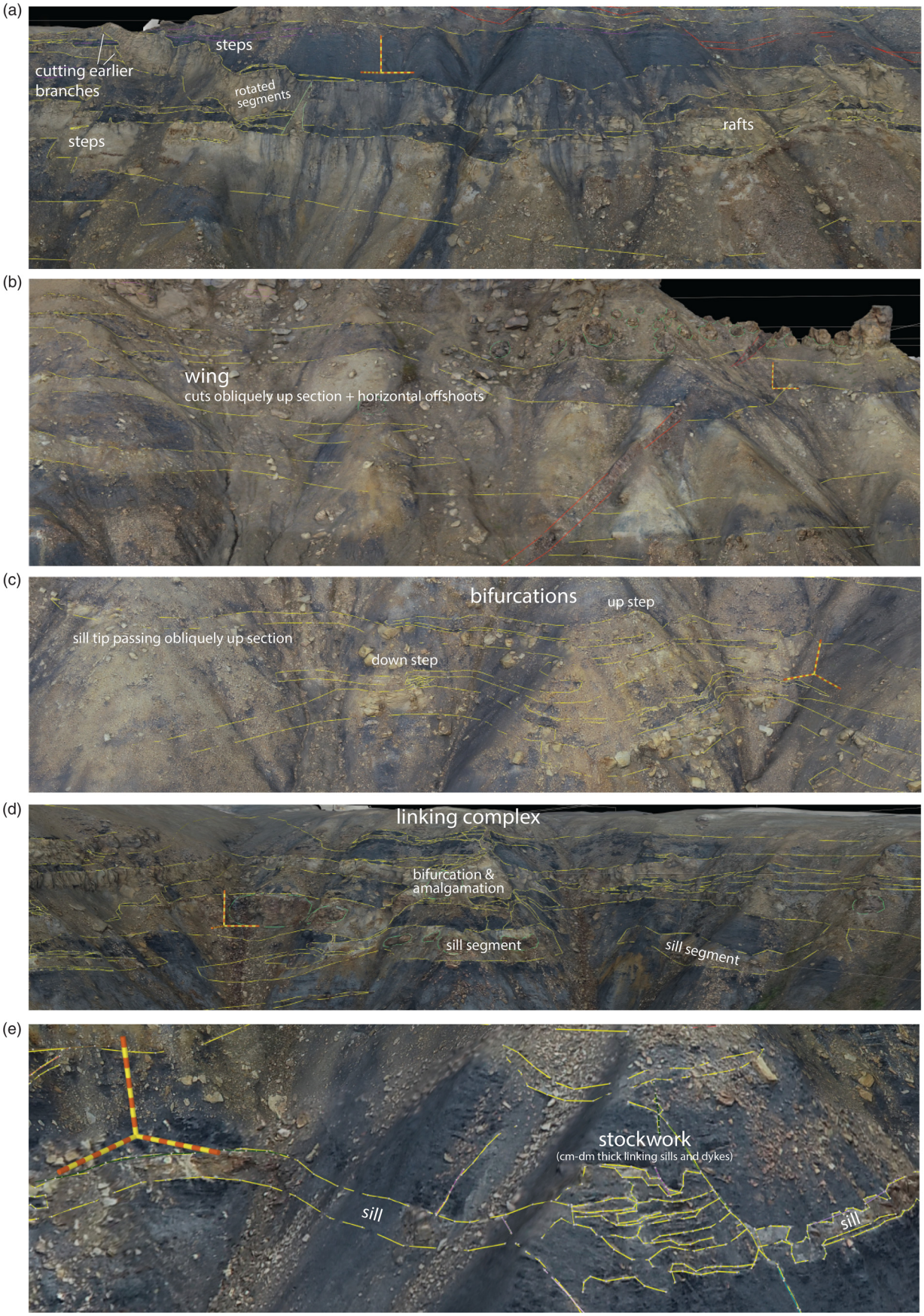

Fig. 5. Interpreted outcrop examples of the commonly identified features in the remobilized sand bodies. (**a**) Steps and host rock rafts, (**b**) wings, (**c**) bifurcations, (**d**) linking complexes and (**e**) stockworks. Scale bars are 10 m, with 1 m increments. See Figure 4 for the position of each element.

Sand body 12

Sand body 12 extends for 900 m and reaches a maximum thickness of 22 m (Fig. 4h). The base of sand body 12 is largely planar, but tends to pass obliquely up the stratigraphy towards the unit margins, where the sand body thins and bifurcates. The upper contact is somewhat complicated by intervals of amalgamation with a westwards extension of sand body 9 (not fully described because it forms the cliff top and appears to have been partially eroded out). The amalgamation surface is defined by a horizon of large-scale mudstone rafts up to 40 m long and 14 m thick. The eastern margin of sand body 12 displays simple thinning and bifurcation. A similar trend is observed towards the western margin; however, this is allied with the presence of a complex array of mudstone rafts and sandstone dykes that link the blocky sandstone elements. The complexity observed at this margin may be related to the proximity of another sandstone body that is partially exposed to the west. The zone of maximum complexity coincides with where these two sand bodies are linked. Linkages to the overlying sand body 9 are also common in this area and form dykes 5–10 m wide. In one example, multiple off-shooting sills are associated with a linking vertical intrusion, alongside areas of stockwork sandstone veining.

Decimetre-scale banding is noted within sand body 12, but no ordering of its distribution is noted, with preservation likely controlled by increased cementation. Large (7.5 m diameter) spherical, sphero-cylindrical and irregular nodules are observed in this sand body. The irregular nodules are up to 75 m long and 5 m thick and often appear to link several spherical and sphero-cylindrical nodules. A concentration of nodules towards the central portion of sand body 12 is recognized, but two separate groupings are also recorded in more marginal positions.

Commonalities in sand body geometry

The systematic description of the 12 sand bodies identified highlights several commonalities in their form. These include steps, wings, host rock rafts, bifurcations, linking complexes, stockworks and nodule distribution (Fig. 5). Each of these is discussed in more detail here, as well as the trends in the structural data collected from the 3D model (Fig. 6).

Steps

Steps occur towards the sand body margins and largely step in an upwards direction away from the sand body axis. Two forms are recognized: (1) where the steps display near-vertical offsets (up to 5 m), resembling faulting, but not displacing the host rock; and (2) where sill segments (15 m), occasionally rotated, are linked by ramps (Fig. 5a). In the first form, the offsets are either not recognized in adjacent sand bodies or, where mirroring does occur, the displacements are offset from one another.

Vétel and Cartwright (2010) described stepped geometries from dykes within the Panoche Hills LSIC, where dykes propagate as several segments that become linked as the intrusion progresses to produce a stepped form. Similar geometries have also been recognized in igneous intrusions, with the development of stepped forms attributed to intrusion into more brittle host rocks (Eide *et al.* 2017). However, in the examples described here, few instances are recognized where the individual segments are not linked, as is the case in some instances described by Vétel and Cartwright (2010) and Eide *et al.* (2017). Furthermore, no clear broken bridge nor host rock raft related to such a process is recognized. These differences can likely be accounted for by different stress regimes during injection and differences in the mechanical properties of the host rock and the injecting sand body from those in the cited examples.

Wings

Inclined upwardly cutting low-angle dykes emanating from the edges of more horizontal sand bodies are recognized in several of the sand bodies described, and are prominent in sand bodies 3, 7, 8 and 9 (Fig. 4). These features are often termed wings (MacLeod *et al.* 1999; De Boer *et al.* 2007; Jackson *et al.* 2011; Satur *et al.* 2021). They are up to 25 m thick and extend upwards vertically over 40 m (e.g. Fig. 5b). In most examples, bifurcation of the sand body is associated with these wing-like features, with the bifurcations often extending horizontally.

Wing-like intrusions associated with massive sandstone bodies were first described from the Hareelv Formation (Surlyk 1987), but were relatively small-scale features and largely concordant with bedding. In the subsurface, wing-like components are a characteristic feature of sandstone intrusions, where they tend to be inclined tens of degrees, are 10–40 m thick and extend vertically for 50–250 m (Huuse *et al.* 2007). Those described here appear consistent with the scale of subsurface examples, but highlight some of the complexity that would not be resolvable in seismic reflection datasets. Waltham *et al.* (2025) highlighted the abundance of sub-seismic elements in wing complexes described from the San Joaquin Basin, but the relationship of these thinner (<3 m) intrusive networks with the larger wing features is unclear. Similarly, intensely intruded networks are not recorded in association with the wings described here.

Host rock rafts

Host rock rafts, ranging from a few decimetres to >100 m long, are common in several of the described sandstone bodies and are generally distributed along distinct horizons (Fig. 5a), as well as being found towards the margins of the sand bodies. The larger rafts often contain sills and dykes, which, in some instances, appear to delineate incipient break-up and continued raft fragmentation, bridging between the sandstone elements above and below. Trains of smaller fragments of host rock rafts in the proximity of larger rafts provide further evidence of such progressive break-up. The rafts themselves can remain tabular, with angular boundaries, or display a more undulatory character indicative of plastic deformation.

Where found towards the margins of sandstone bodies, these rafts are interpreted to be the product of stoping, where sand has injected along fractures in the adjacent host rock, ultimately incorporating large rafts, as was suggested by Surlyk and Noe-Nygaard (2001) for small-scale host rock rafts. Where rafts are distributed along distinct horizons within thicker sand bodies, they most likely reflect the surfaces along which sandstone intrusions have amalgamated during remobilization. This is often demonstrable where the raft horizons transition laterally into *in situ* host rock that separates two sandstone bodies (Fig. 5a).

Bifurcations

Bifurcations are commonly developed towards the lateral terminations of the sand bodies described. The bifurcations reach up to 200 m in lateral extent, contribute to an overall thinning of the sand body, and commonly cut obliquely up the stratigraphy (Fig. 5c). Both up-stepping and down-stepping branching are noted, with the former being more common. One well-exposed example appears to display a cross-cutting relationship with earlier bifurcations, passing upwards to circumvent abandoned branches (Fig. 5a). The abandonment of branches would require a substantial drop in pressure in the branch that becomes abandoned, potentially possible through a loss of pore pressure via the host rock or to another permeable body, or an overall loss of pressure in the system (Vétel and Cartwright 2010). A period of several days would be needed for

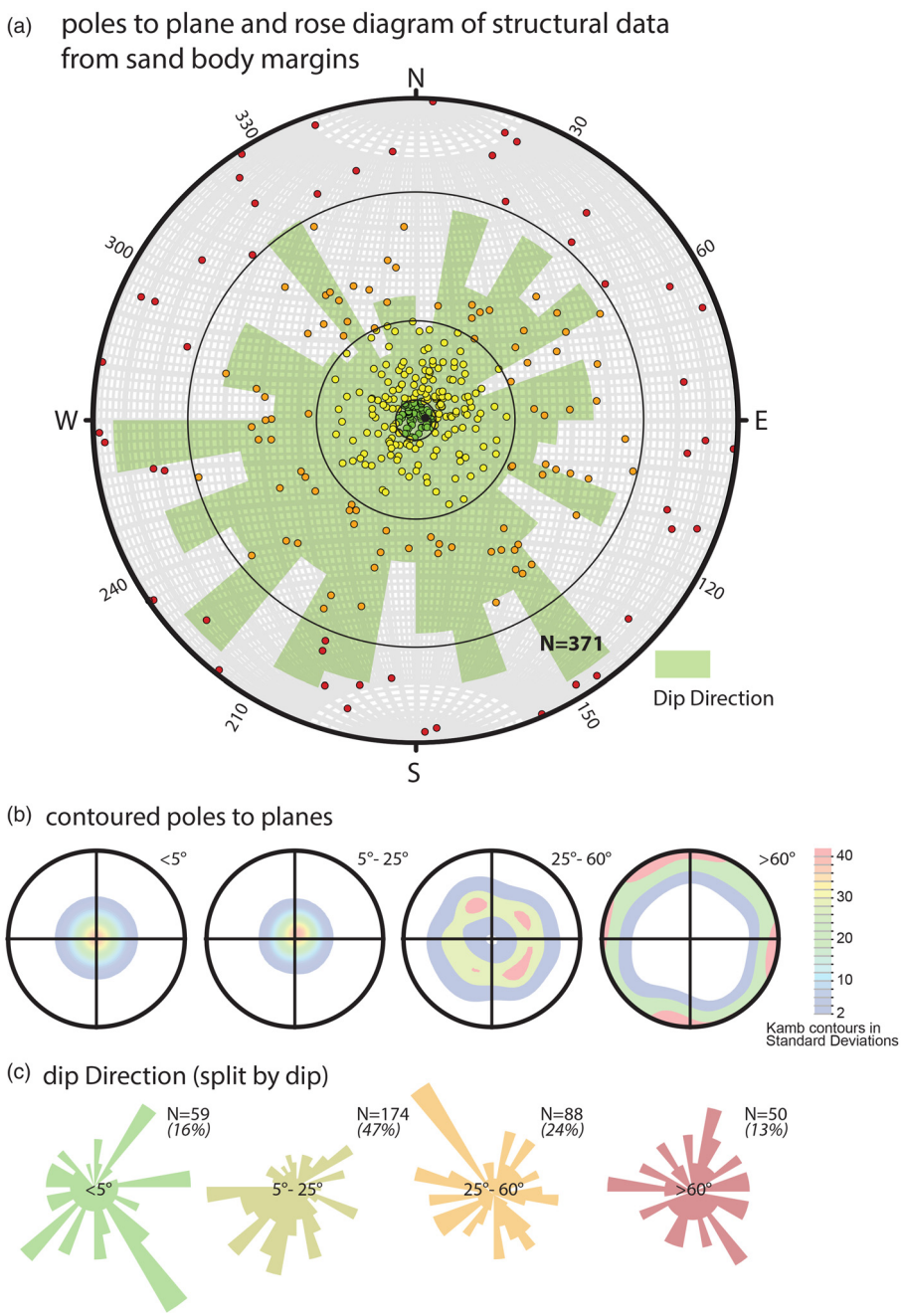

Fig. 6. Structural data from sand body margins in the Hareelv Formation exposed in Ugleelv. (**a**) Data plotted as poles-to-planes, coloured for <5° (green, flat-lying/sills), 5–25° (yellow, sills), 25–60° (orange, oblique dykes) and >60° (red, steep dykes) and underlain by a rose plot of the same data (dip direction). (**b**) Contoured plots of the poles-to-plane data, split in the same divisions as part (a). (**c**) Rose diagrams of the same data, split as in part (b). The regional dip is <3° to the WSW.

one intruded sand body to develop sufficient strength to allow it to be cut by a later intrusion, as suggested by Vétel and Cartwright (2010). The described relationship therefore requires multiple phases of intrusion. This situation could easily be accounted for by multiple large-scale sand bodies intruding at different times and developing linkages with each other.

Linking complexes

Interactions between the described sand bodies occur towards their lateral extents, where the sand bodies thin and a complex array of dykes and sills is often developed (Fig. 5d). Bifurcation and amalgamation occur around large, and sometimes fragmented, host rock rafts that have been created by the emplacement of the surrounding intrusions. Sand body elements often terminate abruptly, or cut steeply upwards, into the overlying units, and a wide array of decimetre- to metre-scale high- and low-angle dykes links the sand body elements. Potential isolated intrusion segments are also tentatively identified in these areas (see towards the base of Fig. 5d). However, if the propagation of the sandstone sills was predominantly through segmented intrusion, then it might be expected that such features would be more readily observed across the outcrop area.

The complexity of the intrusive features identified in these zones likely arises from the dynamic interactions of overpressured sands as liquefaction and injection occurred. This arrangement would have led to rapid changes in pressure as the separate sand bodies connected through injection, resulting in the freezing of some branches and re-routing of the intrusion if pressure was lost, or potentially increased expansion and propagation if the pressure was rapidly increased.

Stockworks

Networks of centimetre- to decimetre-scale sandstone injections have previously been described by Surlyk and Noe-Nygaard (2001) and Surlyk *et al.* (2007), where they were noted to display an orthogonal arrangement, following incipient jointing developed

within the host mudstones. Similar networks have been recognized here, often dominated by injections parallel to bedding and with the linking subvertical elements displaying more variation in orientation. In the present study, these networks tend to be found linking sill segments (Fig. 5e), as well as forming a component of the linking complexes already described. Their localized development between intrusive bodies suggests that the stockworks formed as a response to the proximity of the intrusive bodies to each other. It is therefore suggested that stockworks form where two intrusive bodies reach a point where their respective associated pressure gradients begin to interact, resulting in the fine-scale hydrofracturing of the intervening region leading to linkage of the two intrusive bodies. It is likely that if this progresses further, then a more substantial linkage would form, the only evidence for which would be a change in the alignment of the intrusion and the inclusion of a spread of host rock fragments.

Nodule distribution

Large-scale nodules are found in most of the sand bodies (Fig. 4) and tend to be concentrated towards the centre and base of the thickest portion of each unit (e.g. sand bodies 1, 9 and 10). This is consistent with the observation of Surlyk *et al.* (2007), who additionally documented the cement as dominantly ankerite with some calcite. From an onshore borehole through equivalent stratigraphy to the south (Bløkelv-1), Olivarius *et al.* (2018) recognized that intervals containing pervasive ankerite cement (up to 41 wt%) were often found in finer grained sandstones, which also contained an increased organic content. It was suggested that the finer grained sands would have contained more biogenic mud and were therefore the source of a calcitic precursor. Ankerite would have likely replaced the calcite during later burial once iron and magnesium had been liberated during the smectite to illite transition.

It is difficult to reconcile the potential presence of finer grained, muddier sands towards the central portions of the described sand bodies with any of the likely interpretations of their primary deposition. In submarine lobe settings, which is the interpretation of the sandstone units favoured here, coarser sediment tends to be found towards the sand body axis (Bell *et al.* 2018; de Leeuw *et al.* 2018). Fluid flow would likely have been enhanced in these areas during burial and could therefore have resulted in preferential cementation (e.g. Marini *et al.* 2019; Zhang and Qu 2022). The presence of intraclasts or detrital carbonate (Marini *et al.* 2019) may also have played a part, but no evidence for this was observable in the field. Resolving the controls on the nodule distribution in the examined interval will require further investigation.

Structural trends

Structural measurements, derived from the 3D model of the southern cliffs of Katedralen (Ugleelv), were taken from 371 injectite–host boundaries (Fig. 6). These were individually checked to remove any spurious data points. Figure 6a depicts the poles-to-planes coloured for <5° (green), 5–25° (yellow, sills), 25–60° (orange, oblique dykes) and >60° (red, steep dykes), following the main divisions of Boehm and Moore (2002). The regional structural dip is <3° to the WSW. Little, if any, trend is visible in the poles-to-plane data and this is confirmed from the contouring of the different dip sub-divisions (Fig. 6b). A subtle preferred dip to the SW is recognized in the 5–25° (sills) sub-division. This trend is also apparent when the data are plotted as rose diagrams of dip direction, visible in the total plot, but more clearly picked out in the 5–25° (sills) sub-division (Fig. 6c).

The lack of clear trends within the structural data collected suggests that the stress fields were broadly isotropic during remobilization events and no pre-existing fracture network was being exploited by the sand injectites. This would be as expected if the sand bodies were isolated within the host mudstones. The subtle southwestwards trend in the sill (5–25°) population could be explained by a preferential up-dip mobilization direction of the injected sands, which would then pass obliquely up the stratigraphy, producing the distribution of data recognized here. However, the subtle nature of the recognized trend limits the confidence in such an interpretation.

Discussion

Sand body origins

Surlyk (1987) and Surlyk and Noe-Nygaard (2001, 2003) interpreted the Hareelv Formation sand bodies as originating from deep-water, steep-sided gully-fills. They suggested that the gullies were formed through retrogressive slumping and were later filled with deep-water sands. Although some steep-sided sand bodies are identified in the present study, a lack of clear interaction with the underlying mudstones is striking, with no evidence for erosion. Moreover, no example of remobilized mudstone units is recognized. It is also problematic to consider a mudstone substrate that had the competence to sustain steep gully walls and yet could be loaded into and be compacted by 30–50%, as suggested by Surlyk and Noe-Nygaard (2001). It should, however, be noted that the compaction estimates are made based on intrusions that are described as displaying ptygmatic folding.

The example provided by Surlyk and Noe-Nygaard (2001, their fig. 14) appears instead to illustrate a dyke with an abrupt change in direction, diverting to follow bedding before being deflected as it cuts a sill, and which lacks the linked folds indicative of ptygmatic folding. It is therefore more likely that these features formed at depth when the host mudstones had already undergone substantial compaction rather than from shallow injection, which would have been likely to breach and extrude onto the seabed. Although the generation of high aspect ratio erosional relief at the base of all the sandstone bodies cannot be ruled out, the data presented here favour a more tabular geometry for the sand bodies that were later remobilized. Many of the steep-sided features can be accounted for as wings to the injected sand bodies. Defining the extent of the original (protolith) sand bodies is, however, problematic due to the wholesale remobilization of each unit and the amalgamation/linking of multiple units.

Internally, many of the sand bodies are structureless, although banding is recognized in some examples (e.g. sand body 1, Fig. 4). This was interpreted as flow banding or consolidation laminae by Surlyk *et al.* (2007), forming through gravitational collapse of the grain framework during consolidation shortly after deposition (Hurst and Cronin 2001). It is notable that the banding, as described here, is largely horizontal to sub-horizontal and abuts steeply inclined sand body margins. Such a relationship suggests that the banding formed post-remobilization. The development of banding in only a few areas could be related to an elevated clay/fines content (Lowe 1975; Hurst and Cronin 2001), but detailed thin section analysis is required to test this hypothesis.

Sand bodies of similar textural character and geometry are found up-system on Olympen (Fig. 1) in the Athene Member of the Olympen Formation (Fig. 4i). These sand bodies are often massive and have been interpreted as base of slope fans/lobes (Larsen and Surlyk 2003; Bruhn and Surlyk 2004). It is striking that the gully-fills documented from the upper Hades Member of the Olympen Formation are much smaller in scale (Fig. 4i) than those suggested by Surlyk and Noe-Nygaard (2001, 2003) to act as the protolith sands in the Hareelv Formation. Furthermore, the Hades Member sandstones are observed to have a concentration of carbonaceous

material much higher than that observed in the basin floor fans of the Athene Member and far exceeding what is observed in the Hareelv Formation sands, suggesting that these features were acting as very proximal conduits within the system.

The lack of common and clear erosive bases and the similarity to the base of slope lobe complexes described from the Athene Member, in both scale and textural character, also favours an interpretation of the protolith sand bodies in the Hareelv Formation as lobe complexes. The sourcing of the flows from shelf margin failures, as suggested by Surlyk and Noe-Nygaard (2001, 2003), and the lack of associated sand-filled channel systems would favour the resultant sand bodies being disconnected lobes (*sensu* Brooks *et al.* 2018), aiding the development of overpressure. That said, it is possible that some of these sand bodies may have had connections in the third dimension that are not observed here. Although it cannot be ruled out that the sand bodies are entirely intruded from an original location in the sub-crop, no evidence for remobilization or injection is recognized in the underlying stratigraphy. Furthermore, their high aspect ratio geometry is consistent with them originating as isolated, or only partially connected, submarine lobe complexes. Applying Occam's razor therefore leads to the conclusion that these were probably *in situ* submarine lobes that underwent remobilization.

The level of isolation of the original sand bodies has implications for the development of overpressure and the subsequent evolution of the injectite complex. Because the Hareelv Formation sandstone bodies have undergone wholesale remobilization and injection, it is not possible to ascertain where and if any pre-existing connections were present. Similar deep-water lobe complex sandstones described from the Northern North Sea (Steventon *et al.* 2021) are documented to act as individual pressure cells. If linkages between some of the sand bodies described here did exist prior to remobilization, it may have led to multiple sand bodies injecting at one time.

It is noteworthy that, despite their similarity to the injected sand bodies of the Hareelv Formation, no remobilization is developed in the Olympen Formation. This may be explained by the siltier, bioturbated nature of the encasing mudstones, as described by Larsen and Surlyk (2003) and Bruhn and Surlyk (2004).

Process: a revised model

Surlyk and Noe-Nygaard (2001) provided a thorough review of the potential causes, and trigger mechanisms, for fluidization, highlighting the role of seismic activity in an actively rifting basin. The impact of slope shear stress, slumping, loading, the addition of pore waters from compacting muds and the possibility of thermogenic gas migration were also considered as potentially important in building overpressure. It is, however, difficult to accommodate multiple phases of overpressure generation, as proposed in the model of Surlyk and Noe-Nygaard (2001), to account for cross-cutting relationships, particularly at the shallow depths of burial suggested (tens of metres). It would be expected that intrusion at such depths would reach the seabed, releasing all pressure, but no extrudite has been identified in the exposed overlying stratigraphy. Some of the cross-cutting relationships could be better explained by the interaction of overpressured sand bodies, as discussed for linking complexes, rather than multiple generations of overpressure development and injection. A similar process of interacting intrusion complexes was suggested for the cross-cutting relationships observed in the PGIC (Vétel and Cartwright 2010).

The shallow depth of burial at which Surlyk and Noe-Nygaard (2001) suggested remobilization occurred is consistent with the synthetic models presented by Jolly and Lonergan (2002) and Vigorito and Hurst (2010). These models suggest that self-sourced injectites, dominated by lateral intrusion, occur at depths of centimetres to 10 m, where lithostatic pressure is low. However, as discussed earlier, the evidence for shallow depths of emplacement is questionable. Furthermore, the upwards extension of the intruded wings of the sandstone bodies described here provides a minimum overburden of 40 m. The linking of intrusions with the overlying sand bodies, which must have been present at the time of intrusion (e.g. Fig. 4e, f), further extends this minimum to 100–150 m, indicating that this system developed at far greater depths.

No evidence for extrudites has been reported at any level in the *c.* 400 m thick Hareelv Formation and no injectite system is recognized in the overlying exposures of the Raukeelv Formation (400 m) or the Hesteelv Formation (120 m). The absence of extrudites, and therefore a link to the seabed (i.e. open systems *sensu* Cobain *et al.* 2015), suggests that the Hareelv Formation sand bodies acted as a closed system (*sensu* Cobain *et al.* 2017). Links to deeper sediment source units are also absent, with the underlying Pelion Formation sandstone displaying a sharp unit top, a consistent thickness across the studied region and no evidence for disruption. The underlying stratigraphy may, however, have acted as a source for fluid migration that contributed to the development of overpressure in the Hareelv Formation sand bodies through vertical pressure transfer (e.g. Grauls and Baleix 1994; Tingay *et al.* 2007).

Lateral intrusion is dominant in the Hareelv Formation, requiring the overpressure to exceed the overburden load (lithostatic pressure) (Vétel and Cartwright 2010). The subtle preferential up-dip mobilization direction of the injected sands (Fig. 6), identified from structural data, may point towards lateral pressure transfer also playing a part in building overpressure (e.g. Cartwright 2010). Preferential injection along the up-dip margins of basin floor lobe complexes, where the fluid pressure would be focused and the confining pressure would be at its lowest, has also been documented by Cobain *et al.* (2017). The eastwards progradation of the *c.* 400 m thick Raukelv Formation from the western basin margin during the Volgian (Surlyk *et al.* 1973, 2021; Surlyk and Larsen 2023) may have further contributed to the development of overpressure and encouraged lateral pressure transfer to the up-dip extremities of the Hareelv Formation sand bodies.

A similar driver of overpressure was reported for Oligocene injectites from the eastern North Sea by Andresen and Clausen (2014). However, to overcome lithostatic pressure by lateral pressure transfer alone, it would have to occur rapidly, which is thought to be difficult to achieve (Cartwright 2010). The addition of fluids through vertical migration is a process that may occur rapidly enough to trigger fluidization (Hurst *et al.* 2011). Such a process can be triggered by tectonic activity. Jonk (2010) highlights the likelihood of the interplay of multiple factors in leading to sand remobilization and injection. Such a situation is envisaged here, with no evidence available to attribute injection to a single trigger mechanism.

Evidence for cross-cutting relationships in the Hareelv Formation injectites suggests that multiple phases of intrusion occurred. This could be achieved through the buffering of individual injection pathways during a single event, resulting in individual sills or dykes cutting those that had made more rapid progress through the subsurface, as suggested for the PGIC by Vigorito *et al.* (2022). Such relationships could also occur by the repeated migration of externally sourced fluids, resulting in re-pressurization and multiple phases of sand body injection. If the observed sand bodies are disconnected lobe complexes, without initial connections between them, then they would act as individual pressure cells.

Interactions between multiple isolated cells during phases of injection might be expected to increase the architectural complexity of the resultant injectite system. In this situation, the potential for greater temporal separation between phases of injection is also possible because each sand body could act independently of those around it. However, if several sand bodies were connected initially, and were thus in pressure communication, it might have resulted in

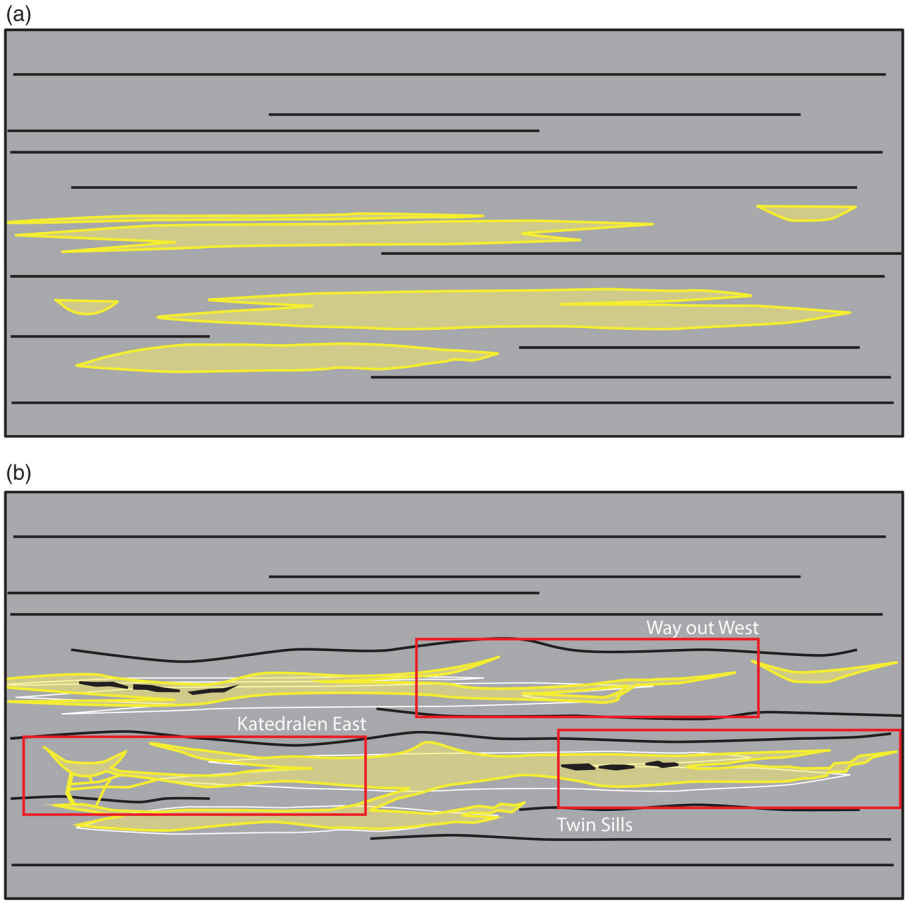

Fig. 7. Revised model for the deposition and remobilization of the Hareelv Formation sand bodies. (**a**) Deposition of large-scale (1–2 km × 50 m) deep-water submarine lobe systems encased in organic-rich, largely non-bioturbated mudstones. (**b**) Overpressure develops, potentially increased due to fluid migration (e.g. iron-rich fluids expelled from the encasing mudstones leading to the development of ankerite nodules in the axial portions of the lobes), together with lateral, and probable vertical, pressure transfer. These processes trigger fluidization of the overpressured sands, which results in the lithostatic pressure being surpassed and pervasive lateral injection. The white lines in part (b) illustrate the original sand body geometries, host rock rafts are in black and the labelled red boxes provide references to examples from the described sections.

several units injecting simultaneously. The limitations of the outcrop and the disruption caused by subsequent remobilization and injection do not allow the potential pre-existing connectivity of the protolith lobe complexes to be fully assessed, but as time progressed the individual sand bodies clearly developed linkages, and these may have influenced subsequent re-pressurization and wider interactions during injection. The potential for such repeated pressurization would likely be far more characteristic of closed systems such as this, in contrast with systems open to the surface.

To satisfy the observations and inferences that have been made, the Hareelv sandstone intrusions are interpreted as submarine lobe complexes that acted as self-sourced and closed systems, dominated by lateral injection with remobilization occurring at burial depths >150 m, but potentially much deeper (cf. the several hundred metres of Cobain *et al.* 2017). Such a model can accommodate the range of geometries and features described (Fig. 7).

Injectite distribution

At outcrop, remobilization appears ubiquitous within the sandstones of the Hareelv Formation. However, it is notable that remobilization and injection are not recognized in the age-equivalent Olympen Formation (Larsen and Surlyk 2003; Bruhn and Surlyk 2004) and is also of a lesser prominence in the Lollandselv-1, Lollandselv-2 and Fasterelv-1 core penetrations (SW Jameson Land, Fig. 1) of the Hareelv Formation (Bjerager *et al.* 2018). By contrast, the southernmost core through the Hareelv Formation (Blokelv-1) displays evidence for remobilization in most of the sandstones penetrated (Bjerager *et al.* 2018). The key differentiation between those core penetrations and outcrop examples that are widely affected by remobilization and those that are not affected is the siltier nature of the host mudstones and the presence of bioturbation in the examples with limited injection. The coarser grain size and the presence of bioturbation is likely to have impacted the sealing capacity and therefore the potential to build overpressure in the encased sandstones. Taken in the context of the geographical distribution of the outcrops and boreholes discussed, it seems likely that this distinction can further be attributed to proximal–distal relationships, with a higher sediment supply and oxygenation levels towards the basin margins.

Comparisons and subsurface examples

The intensively studied PGIC developed under a contractional tectonic regime and is dominated by dyke complexes, with the development of sills restricted to discrete intervals (Vigorito *et al.* 2008; Vétel and Cartwright 2010). The sill complexes described from the PGIC consist of sets of relatively thin (15 m) sills (Vigorito *et al.* 2008; Zvirtes *et al.* 2020), which, despite displaying several similarities in geometry, are very different from those described herein and from subsurface datasets from the North Sea Basin LSIC (e.g. Duranti *et al.* 2002; Huuse *et al.* 2004; Andresen and Clausen 2014) (Figs 4j, 8). It should also be noted that the PGIC examples are observed to have formed as part of an open system with extrudites (Vigorito *et al.* 2008; Vétel and Cartwright 2010).

By contrast, there is no evidence for extrudites in the Hareelv Formation examples. Similarly, there is often limited evidence to suggest that the examples described from the North Sea Basin reached the seabed, although the presence of extrudites has been postulated in some examples (e.g. Huuse *et al.* 2005; Hurst *et al.* 2006; Løseth *et al.* 2012, 2013). In particular, it is noted that the origin of the large-scale examples highlighted by Løseth *et al.* (2012, 2013) has been strongly disputed (Rundberg and Eidvin 2015). Outcrop examples of injectites from the deep-water systems of the Vocontian Basin in SE France are sill-dominated and display some similarities in geometry to those described from the Hareelv

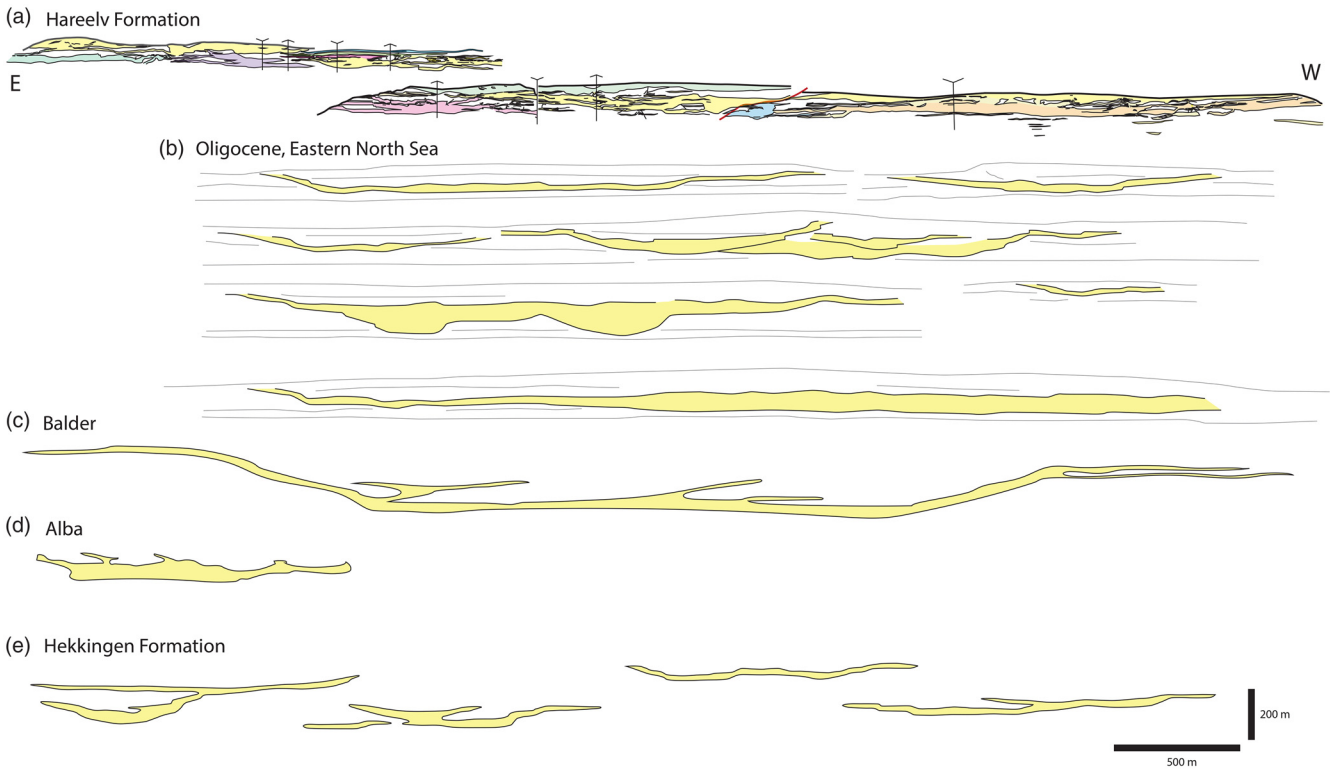

Fig. 8. Comparison of the gross morphology of the sand bodies described from (**a**) southern Ugleelv with similarly scaled subsurface examples from the North Sea: (**b**) the Oligocene of the eastern North Sea (six separate intrusion complexes), interpreted as deeply sourced and emplaced in the shallow subsurface, potentially reaching the seabed; (**c**) the Balder intrusion, south Viking Graben; (**d**) the Alba intrusion, outer Moray Firth; and (**e**) the Hekkingen Formation injectite bodies from the Barents Shelf. All the examples have had any vertical exaggeration removed. Note that, in part (a), the exact scale varies across the component panels due to the relief of the cliff sections; see Fig. 4 for the colour key. Source: part (b) modified from Andresen and Clausen (2014); part (c) modified from Huuse *et al.* (2004); and part (d) modified after Duranti *et al.* (2002).

Formation (Parize and Friès 2003; Parize *et al.* 2007), but their relatively limited extent and proposed mode of emplacement are markedly different.

Given the difference in the evolution of pressure regimes between open and closed systems, it would be expected that several differences in the architecture of the resultant injection complexes would exist. One clear difference between the open PGIC system and the closed Hareelv Formation LSIC system described here is the dominance of dykes and large-scale sills, respectively (Fig. 4). The subsurface examples illustrated in Figure 8 range from 500 m to 5 km in lateral extent and *c.* 20–80 m in thickness. Obliquely oriented margins/wings that rise through 40–200 m of stratigraphy are common and, in some instances, these appear to show a stepped form. Bifurcations are also recognized towards the lateral extremities of the sand bodies, as well as forming splays from the top of the sand bodies. The scale of the Hareelv sand bodies, up to 2 km in lateral extent and 50 m thick, is strikingly similar to those described from the subsurface, as are the range of macro-scale features/geometries that they display.

The confident identification of source units and feeder systems to large-scale injectite systems in subsurface datasets is often problematic (Andresen and Clausen 2014; Cobain *et al.* 2021), but has been achieved in some instances (e.g. Duranti and Hurst 2004; Shoulders and Cartwright 2004). Vigorito and Hurst (2010) also noted the difficulty in tying source units to intrusive bodies in subsurface datasets. The similarity of the subsurface examples described here (Fig. 8) and the self-sourced injectite sand bodies of the Hareelv Formation highlights that the need for a more distant source and associated conduit system may be the exception rather than expectation. Such a situation is aligned with examples from the Harding and Alba fields described by Jolly and Lonergan (2002), but contrasts with their generic models (their fig. 2) and those from Hurst *et al.* (2011), highlighting the value that the Hareelv Formation dataset can bring to developing more widely applicable, and predictive, models.

Comparisons with unpublished subsurface data from the Late Jurassic to Early Cretaceous injectite systems from the UK and Norwegian continental shelves (the East Shetland Basin, e.g. the Magnus, Cladhan and Home sandstones; the Outer Moray Firth, e.g. the Polecat, Martin, Honey Badger, Ettrick and Buzzard fields; the Brae area, UK sector; the South Viking Graben, Norwegian sector, e.g. the Gudrun and Harry Klein fields; the North Viking Graben, Norwegian sector, e.g. the Lomre Terrace; Mid-Norway, e.g. Fenja to Bremstein; and the Barents Sea, e.g. the Hekkingen Formation and the western and southern flank of the Loppa High) highlight several commonalities.

These subsurface examples extend from the UK Moray Firth to the Norwegian Barents Sea and were deposited as part of the same evolving North Atlantic rifted seaway under the same climatic, rift phase and relative sea-level trends as the Greenland examples (Fig. 2). Core and seismic reflection data from these areas highlight that gravity-flow sands (slope channel-fills, channelized lobes and basin floor fans) encased within non-bioturbated anoxic to dysoxic, organic-rich source and seal mudstone units of Oxfordian–Berriasian age (e.g. Hoth *et al.* 2018; Jones and Van Bergen 2018; Turner *et al.* 2018; Tillmans *et al.* 2021; Brekke *et al.* 2025; Brunstad and Rønnevik 2025) are more prone to remobilization and injection than the gravity-flow sands that are interbedded with more heterolithic, silty, oxygenated and bioturbated facies that typify the Bathonian and Callovian (Copestake and Partington 2023; Brekke *et al.* 2025; Brunstad and Rønnevik 2025). These super-regional observational data suggest a causative link between the encasing organic-rich high total organic carbon (TOC) mudstone facies and the injection process.

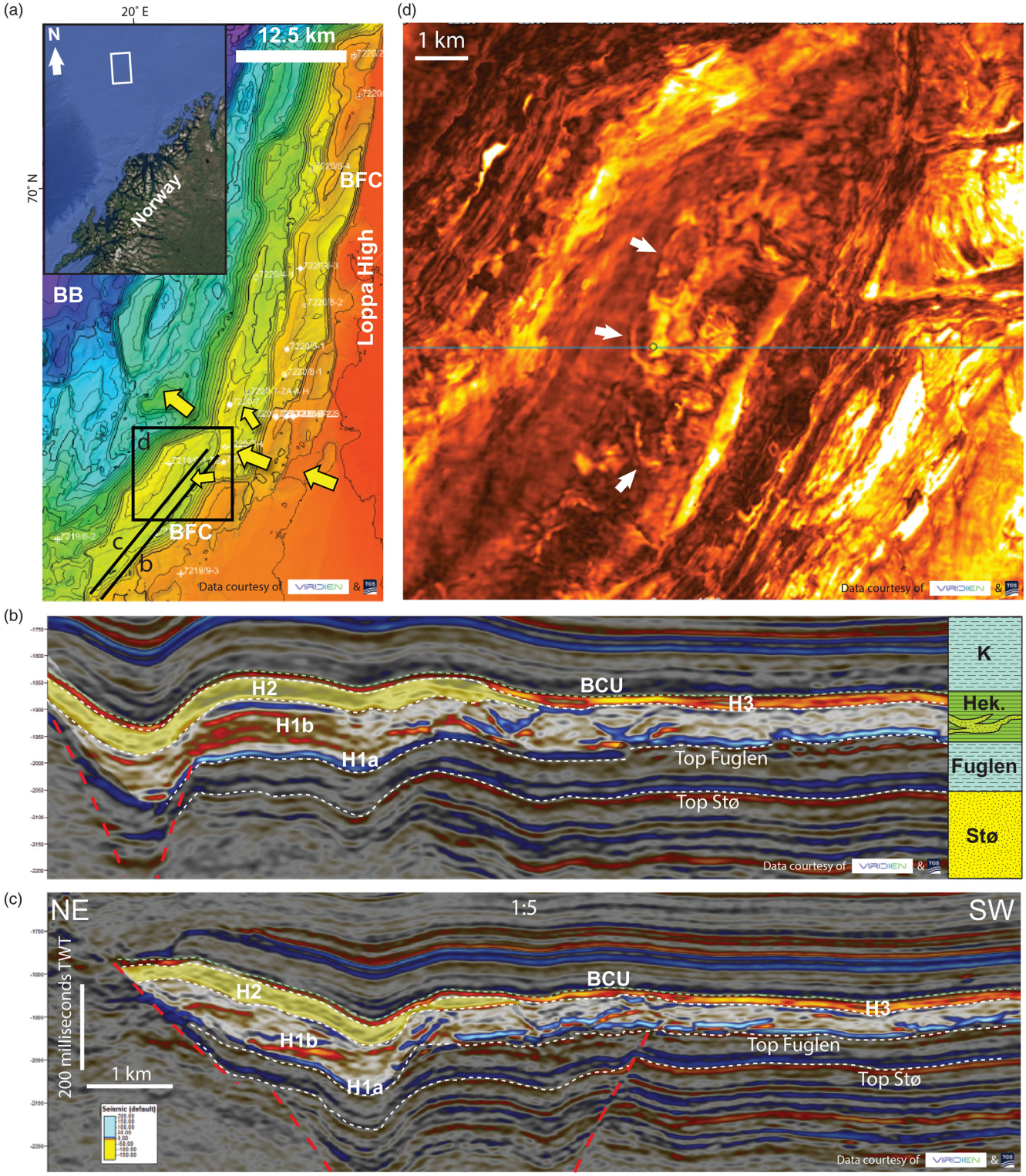

Fig. 9. A subsurface injectite complex in the Late Jurassic of the Barents Shelf. (**a**) Two-way travel time seismic surface map of the base Cretaceous unconformity highlighting Late Jurassic–Early Cretaceous NNE–SSW-striking rift phase faults and half-graben/fault blocks developed along the western edge of the Loppa High (inset shows the location). The position of the seismic reflection lines illustrated in parts (b) and (c), and the position of the RMS horizon slice provided in part (d), are indicated. The main sediment input points during the Late Jurassic are illustrated by yellow arrows. BB, Bjørnøya Basin; BFC, Bjørnøyrenna Fault Complex. Well control points are indicated in white text. (**b**, **c**) Seismic reflection lines (ms TWT) (1:5) illustrating the seismic stratigraphic units and the geometries and the strata-bound nature of the injectite sand bodies (blue) within the unit H1b division of the Hekkingen Formation. The interpreted main sediment input direction is from the NE (left) on both images. Note the development of the overlying unit H2 sand package (shaded light yellow), which thins into the basin and may have contributed to the development of overpressure within the underlying sand bodies. The stratigraphy is provided in part (b), K, Cretaceous, Hek., Hekkingen Formation, and the key to the lithologies can be found in Figure 3. (**d**) Intra-Hekkingen Formation RMS amplitude extraction horizon slice (±12 ms) created using Petrel (Schlumberger; SLB 2022) and PaleoScan™ (Eliis 2019) software. The arrowed semi-circular features represent hard impedance geobodies, here interpreted as partly carbonate-cemented injected sands within unit H1b, as illustrated in parts (b) and (c). These features highlight the ovoid nature of the injectite sand bodies and associated wings (arrowed high amplitudes) that climb and step through stratigraphy towards the SW. The seismic cube utilized is CGG19002-KPSDM-FINAL-FULL-STK-0-35-TIME from Viridien (formerly CGG) and TGS.

Using well, core and biostratigraphically tied 3D seismic data from the Barents Shelf (Fig. 9a) as a case study, major strata-bound injectite complexes have been mapped encased within organic-rich shales of the Hekkingen Formation (Fig. 9b, c). The Hekkingen Formation overlies the Oxfordian–Callovian–Bathonian bioturbated shelfal hetrolithics and Bajocian–Aalenian shelfal sands of the Fuglen and Stø formations, respectively (Fig. 9b, Sollid *et al.* 2021; Ryseth *et al.* 2025), a situation directly comparable with the East Greenland outcrops. The base of the Hekkingen Formation is characterized by a 10–30 m thick, regionally extensive, high-TOC shale succession of Kimmeridgian–Early Tithonian age (unit H1a, base seal unit; Tripathy *et al.* 2018; Jelby *et al.* 2020; Cedeño *et al.* 2021).

On seismic reflection and well data, the overlying main part of the Hekkingen Formation can be further subdivided into a lower (unit H1b), regionally extensive, 30–90 m thick, high-TOC mudstone unit with well-imaged interbedded injected sands and a distinct capping higher TOC-rich shale, an upper 10–70 m thick homogenous, but locally developed, sand-dominated unit (unit H2) and a capping regionally extensive 10–20 m thick hot shale unit (unit H3) with localized injected sands of Berriasian age (Fig. 9b, c). There is a clear spatial relationship in the thickness and facies of the H1b and H2 intervals to rift margin point-sourced feeder canyons (Fig. 9a), with well, amplitude v. offset and seismic geomorphology data confirming a higher percentage of sandstone, particularly in unit H2, immediately outboard of the feeder canyons, and a gradual loss in sand content moving radially away from the point-sourced feeders (Fig. 9b, c). In seismic sections, the lower H1b unit is characterized by well-imaged discordant bright injectite wings with complex cross-cutting relationships (Fig. 9b, c), whereas unit H2 is seismically more transparent.

Individual injectite wing geobodies within unit H1b are between 500 and 750 m long on average, but can extend up to 1.5 km long, and tend to step up and away from depositional thicks of unit H2 (Figs 9b, c and 7e). Individual wings are imaged to pass obliquely upwards or form distinct steps, cutting over 20–50 m of vertical stratigraphy. In seismic map view, the injectite wing features within unit H1b have both semi-circular and elongate long axis forms and have a predominance of convex outer edges facing away from the main thicks of unit H2 (Fig. 9d). Dip and strike seismic sections moving away from identified point-source feeder canyons indicate a gradual loss of injectite geometries and a corresponding loss of net to gross, passing into the sheet-like, homogenous, mudstone-dominated Hekkingen Formation facies (Fig. 9b, c), which at a basin scale are more typical of this interval (e.g. Cedeño *et al.* 2021). Collectively, the well-tied seismic observations indicate a close link between the main sediment input point/thicks and the injectite complex development, with a possible genetic link between sediment loading by unit H2 (Fig. 9b, c, pale yellow coloured unit) and injection within unit H1b.

It is worth noting that production well and seismic reflection data in the study area indicate that the Stø and Fuglen formations are sheet-like and homogenous (Sollid *et al.* 2021) and that the main injectite complex is intra-formational and strata-bound, confined within the Hekkingen Formation (Fig. 9b, c), developing immediately above the basal hot shale and not extending above the base Cretaceous unconformity. Injectite features have not been observed extending upwards from the Stø Formation, developed within the Fuglen Formation nor extending down from the Hekkingen Formation. This situation compares well with the East Greenland outcrop observations. Locally, the Top Fuglen Formation to Hekkingen Formation contact does show seismic evidence for some disturbance/block gliding and 'pop-up'-like structures, with a clear spatial relationship of these features with the thickest and more sand-dominated Hekkingen Formation immediately outboard of the feeder canyons.

In summary, the closed Hareelv Formation LSIC system shares close affinities with age-equivalent examples described here from the Barents Sea (Fig. 9) and several published North Sea examples (Fig. 8) of large-scale injectites, in terms of scale, morphology, architecture and palaeogeographical and tectonic setting. The interpretation of the Hareelv Formation presented here can therefore shift the paradigm that has guided the interpretation of subsurface datasets and offers the opportunity to add valuable sub-seismic scale observations on connectivity, injectite facies and contacts. The Hareelv Formation LSIC may provide a more appropriate analogue for North Atlantic LSICs than the Panoche Hills LSIC.

Conclusions

The Hareelv Formation provides the only outcrop example of a kilometre-scale sandstone intrusion complex in an extensional tectonic setting and is one of very few outcrop examples of an LSIC. Furthermore, it is the only outcrop LSIC example that is interpreted to have developed as a closed system. As such, it is uniquely important in the development of sand injectite models and subsurface prediction. This study has focused on the large-scale geometry of the sand bodies identified within the Hareelv Formation across the superb exposures found in Ugleelv (Jameson Land). Twelve discrete sand bodies, extending for up to 2 km laterally and up to 50 m in thickness, were identified across the 5 km long cliff section using a high-resolution 3D model. Several features were found to be common across the described sand bodies, including steps, wings, host rock rafts, bifurcations, linking complexes and stockworks.

Little evidence was found for the previously postulated presence of widely developed erosive bases and slope gully features. Instead, the broad geometry of the sand bodies and their textural character compares closely with sandstone bodies found within the Olympen Formation (an up-system correlative of the basal Hareelv Formation), which are interpreted as base of slope submarine lobe complexes. A similar origin is favoured here for the Hareelv Formation sandstone bodies, with irregularities largely the product of remobilization. These were probably disconnected lobes, with little evidence for associated sand-filled channel systems, resulting in isolated, or only partially connected, sand bodies suited to the development of overpressure when encased in organic-rich mudstones.

Mobilization and injection occurred in a closed system and was dominated by lateral intrusion at depths >150 m. Fluidization and injection would ultimately have resulted from the interaction of several factors. The subtle preferential up-dip mobilization direction of injected sands, identified from structural data, may point towards lateral pressure transfer playing a part in building overpressure. Sediment loading from the progradation of the Raukelv Formation in the Volgian may also have had a contributory role in building overpressure, alongside potential fluid migration from deeper stratigraphic levels (vertical pressure transfer). The proposed model illustrates the formation of the features described and their relationships to one another. The similarity to subsurface examples, which have often been interpreted to be linked to deeper source intervals, is recognized and it is proposed that many of these may, in fact, be similar in their genesis to the Hareelv Formation examples in being self-sourced and dominated by lateral intrusion in a closed system. The injectite sand bodies from the Hekkingen Formation on the Barents Shelf described here provide an age-equivalent subsurface case study that can be demonstrated to act as a closed system and contains sand body geometries that closely resemble those described from the Hareelv Formation.

The distribution of remobilized sands within the Hareelv Formation of the Jameson Land Basin appears to be influenced by the composition and level of bioturbation of the encasing mudstones/siltstones. Sandstone intrusions are more prevalent in

basinal areas where the encasing sediment contains less silt and was deposited in an oxygen-poor environment where bioturbation was limited. A similar distribution is recognized in the Late Jurassic on the UK and Norwegian continental shelves.

Scientific editing by Alexandra Tamas

Acknowledgements We thank Equinor for supporting this work and Paul Walker for providing logistic support in the field. We thank the reviewers, Joe Cartwright and Rene Jonk, for their constructive comments and Editor Alexandra Tamas for handling the manuscript. We acknowledge Schlumberger for the industry licence for Petrel, Ellis for providing PaleoScan, and Viridien (formerly CGG) and TGS for permission to publish selected examples from 3D seismic reflection data from the Barents Sea CGG19002 3D survey.

Author contributions **SDA**: conceptualization (lead), data curation (lead), formal analysis (lead), investigation (lead), methodology (lead), writing – original draft (lead), writing – review and editing (lead); **EK**: investigation (supporting), writing – review and editing (supporting); **DMH**: funding acquisition (lead), writing – original draft (supporting), writing – review and editing (equal); **JP**: funding acquisition (supporting), writing – review and editing (supporting); **IAK**: funding acquisition (supporting), writing – review and editing (supporting); **BJB**: writing – review and editing (supporting); **IS**: writing – original draft (supporting), writing – review and editing (supporting); **MAS**: formal analysis (supporting).

Funding This work was funded by Equinor.

Competing interests The authors declare that they have no known competing financial interests or personal relationships that could have appeared to influence the work reported in this paper.

Data availability The 3D seismic data that support the findings of this study are available from CGG Services Norway AS, but restrictions apply to the availability of these data, which were used under licence for the current study and are not publicly available. Data are, however, available from the authors upon reasonable request and with permission of CGG Services Norway AS.

References

Agisoft LLC. 2022. Agisoft Metashape (version 2.0.0), https://www.agisoft.com

Andresen, K.J. and Clausen, O.R. 2014. An integrated subsurface analysis of clastic remobilization and injection; a case study from the Oligocene succession of the eastern North Sea. *Basin Research*, **26**, 641–674, https://doi.org/10.1111/bre.12060

Andrews, S.D., Morton, A. and Decou, A. 2021. Middle–Late Triassic evolution of the Jameson Land Basin, East Greenland. *Geological Magazine*, **158**, 930–949, https://doi.org/10.1017/S001675682000093X

Bell, D., Kane, I.A., Pontén, A.S., Flint, S.S., Hodgson, D.M. and Barrett, B.J. 2018. Spatial variability in depositional reservoir quality of deep-water channel-fill and lobe deposits. *Marine and Petroleum Geology*, **98**, 97–115, https://doi.org/10.1016/j.marpetgeo.2018.07.023

Bjerager, M., Alsen, P., Bojesen-Koefoed, J.A., Nielsen, T., Piasecki, S. and Pilgaard, A. 2018. Late Jurassic evolution of the Jameson Land Basin, East Greenland–implications of the Blokelv-1 borehole. *GEUS Bulletin*, **42**, 149, https://doi.org/10.34194/geusb.v42.4325

Boehm, A. and Moore, J.C. 2002. Fluidized sandstone intrusions as an indicator of paleostress orientation, Santa Cruz, California. *Geofluids*, **2**, 147–161, https://doi.org/10.1046/j.1468-8123.2002.00026.x

Brekke, H., Bunkholt, H.S., Faleide, J.I. and Fyhn, M.B. 2025. Definition of tectono-sedimentary elements for rifted continental margins of the Norwegian and Greenland seas. *Geological Society, London, Memoirs*, **57**, 97–102, https://doi.org/10.1144/M57-2021-31

Brooks, H.L., Hodgson, D.M., Brunt, R.L., Peakall, J., Poyatos-Moré, M. and Flint, S.S. 2018. Disconnected submarine lobes as a record of stepped slope evolution over multiple sea-level cycles. *Geosphere*, **14**, 1753–1779, https://doi.org/10.1130/GES01618.1

Bruhn, R. and Surlyk, F. 2004. Sand-grade density flow evolution on a shelf-edge–slope–basin-floor complex in the Upper Jurassic Olympen Formation, East Greenland. *Petroleum Geoscience*, **10**, 81–92, https://doi.org/10.1144/1354-079302-559

Brunstad, H. and Rønnevik, H.C. 2025. Loppa High composite tectono-sedimentary element, Barents Sea. *Geological Society, London, Memoirs*, **57**, 378–397, https://doi.org/10.1144/M57-2020-3

Cartwright, J. 2010. Regionally extensive emplacement of sandstone intrusions: a brief review. *Basin Research*, **22**, 502–516, https://doi.org/10.1111/j.1365-2117.2009.00455.x

Cedeño, A., Ohm, S., Escalona, A., Marín, D., Olaussen, S. and Demchuk, T. 2021. Upper Jurassic to Lower Cretaceous source rocks in the Norwegian Barents Sea, part I: organic geochemical, petrographic, and paleogeographic investigations. *Marine and Petroleum Geology*, **134**, 105342, https://doi.org/10.1016/j.marpetgeo.2021.105342

Cobain, S.L., Peakall, J. and Hodgson, D.M. 2015. Indicators of propagation direction and relative depth in clastic injectites: implications for laminar versus turbulent flow processes. *GSA Bulletin*, **127**, 1816–1830, https://doi.org/10.1130/B31209.1

Cobain, S.L., Hodgson, D.M., Peakall, J. and Shiers, M.N. 2017. An integrated model of clastic injectites and basin floor lobe complexes: implications for stratigraphic trap plays. *Basin Research*, **29**, 816–835, https://doi.org/10.1111/bre.12229

Cobain, S.L., Hodgson, D.M., Peakall, J. and Silcock, S.Y. 2021. Relationship between bowl-shaped clastic injectites and parent sand depletion: implications for their scale-invariant morphology and composition. *Geological Society, London, Special Publications*, **493**, 135–149, https://doi.org/10.1144/SP493-2018-80

Copestake, P. and Partington, M.A. 2023. Sequence stratigraphy scheme for the Middle Jurassic of the North Sea area. *Geological Society, London, Memoirs*, **59**, 99–134 https://doi.org/10.1144/M59-2022-68

De Boer, W., Rawlinson, P.B. and Hurst, A. 2007. Successful exploration of a sand injectite complex: Hamsun prospect, Norway Block 24/9. *AAPG, Memoirs*, **87**, 65–68, https://doi.org/10.1306/1209850M873256

De Leeuw, J., Eggenhuisen, J.T., Spychala, Y.T., Heijnen, M.S., Pohl, F. and Cartigny, M.J. 2018. Sediment volume and grain-size partitioning between submarine channel–levee systems and lobes: an experimental study. *Journal of Sedimentary Research*, **88**, 777–794, https://doi.org/10.2110/jsr.2018.46

Duranti, D. and Hurst, A. 2004. Fluidization and injection in the deep-water sandstones of the Eocene Alba Formation (UK North Sea). *Sedimentology*, **51**, 503–529, https://doi.org/10.1111/j.1365-3091.2004.00634.x

Duranti, D., Hurst, A., Bell, C., Groves, S. and Hanson, R. 2002. Injected and remobilized Eocene sandstones from the Alba Field, UKCS: core and wireline log characteristics. *Petroleum Geoscience*, **8**, 99–107, https://doi.org/10.1144/petgeo.8.2.99

Eide, C.H., Schofield, N., Jerram, D.A. and Howell, J.A. 2017. Basin-scale architecture of deeply emplaced sill complexes: Jameson Land, East Greenland. *Journal of the Geological Society, London*, **174**, 23–40, https://doi.org/10.1144/jgs2016-018

Eliis, 2019. Paleoscan (version 2019.2), www.eliis-geo.com/paleoscan/

Grauls, D.J. and Baleix, J.M. 1994. Role of overpressures and in situ stresses in fault-controlled hydrocarbon migration: a case study. *Marine and Petroleum Geology*, **11**, 734–742, https://doi.org/10.1016/0264-8172(94)90026-4

Henriksen, N. 1984. *Geological Map of Greenland, 1:500 000, Sheet 12, Scoresby Sund*. GEUS, https://doi.org/10.22008/FK2/GO6TAW

Hesselbo, S.P., Ogg, J.G., Ruhl, M., Hinnov, L.A. and Huang, C.J. 2020. The Jurassic period. *In*: Gradstein, F.M., Ogg, J.G., Schmitz, M.D. and Ogg, G.M. (eds) *Geologic Time Scale 2020*. Elsevier, 955–1021.

Hodgetts, D., Seers, T., Head, W. and Burnham, B.S. 2015. High performance visualisation of multiscale geological outcrop data in single software environment. Paper presented at the 77th EAGE Conference and Exhibition, 1–4 June, Madrid. European Association of Geoscientists and Engineers, https://doi.org/10.3997/2214-4609.201412862

Hoth, S., Knaust, D., Sánchez-López, A., Kassold, S. and Sviland-Østre, S. 2018. The Gudrun field: gravity-flow deposition during rifting and inversion. *AAPG, Memoirs*, **115**, 387–422, https://doi.org/10.1306/13652188M1153814

Hurst, A. and Cronin, B.T. 2001. The origin of consolidation laminae and dish structures in some deep-water sandstones. *Journal of Sedimentary Research*, **71**, 136–143, https://doi.org/10.1306/061400710136

Hurst, A., Cartwright, J. and Duranti, D. 2003. Fluidization structures produced by upward injection of sand through a sealing lithology. *Geological Society, London, Special Publications*, **216**, 123–137, https://doi.org/10.1144/GSL.SP.2003.216.01.09

Hurst, A., Cartwright, J.A., Huuse, M. and Duranti, D. 2006. Extrusive sandstones (extrudites): a new class of stratigraphic trap? *Geological Society, London, Special Publications*, **254**, 289–300, https://doi.org/10.1144/GSL.SP.2006.254.01.15

Hurst, A., Scott, A. and Vigorito, M. 2011. Physical characteristics of sand injectites. *Earth-Science Reviews*, **106**, 215–246, https://doi.org/10.1016/j.earscirev.2011.02.004

Huuse, M., Duranti, D. *et al.* 2004. Seismic characteristics of large-scale sandstone intrusions in the Paleogene of the south Viking Graben, UK and Norwegian North Sea. *Geological Society, London Memoirs*, **87**, 263–278, https://doi.org/10.1144/GSL.MEM.2004.029.01.25

Huuse, M., Cartwright, J.A., Gras, R. and Hurst, A. 2005. Kilometre-scale sandstone intrusions in the Eocene of the Outer Moray Firth (UK North Sea): migration paths, reservoirs and potential drilling hazards. *Geological Society, London, Petroleum Geology Conference Series*, **6**, 1577–1594, https://doi.org/10.1144/0061577

Huuse, M., Cartwright, J.A. and Hurst, A. 2007. Seismic characterization of large scale sandstone intrusions. *AAPG, Memoirs*, **87**, 21–36, https://doi.org/10.1306/1209847M873253

Jackson, C.A.-L., Huuse, M. and Barber, G.P. 2011. Geometry of winglike clastic intrusions adjacent to a deep-water channel complex: implications for

hydrocarbon exploration and production. *AAPG Bulletin*, **95**, 559–584, https://doi.org/10.1306/09131009157
Jelby, M.E., Śliwińska, K.K., Koevoets, M.J., Alsen, P., Vickers, M.L., Olaussen, S. and Stemmerik, L. 2020. Arctic reappraisal of global carbon-cycle dynamics across the Jurassic–Cretaceous boundary and Valanginian Weissert Event. *Palaeogeography, Palaeoclimatology, Palaeoecology*, **555**, 109847, https://doi.org/10.1016/j.palaeo.2020.109847
Jolly, R.J. and Lonergan, L. 2002. Mechanisms and controls on the formation of sand intrusions. *Journal of the Geological Society, London*, **159**, 605–617, https://doi.org/10.1144/0016-764902-025
Jones, D.W. and Van Bergen, P. 2018. Reservoir geology of the Upper Jurassic Brae Sandstone Member, Kingfisher Field, South Viking Graben, UK North Sea. *AAPG, Memoirs*, **115**, 283–305, https://doi.org/10.1306/13652185M1153812
Jonk, R. 2010. Sand-rich injectites in the context of short-lived and long-lived fluid flow. *Basin Research*, **22**, 603–621, https://doi.org/10.1111/j.1365-2117.2010.00471.x
Larsen, M. and Surlyk, F. 2003. Shelf-edge delta and slope deposition in the upper Callovian–middle Oxfordian Olympen Formation, east Greenland. *GEUS Bulletin*, **1**, 931–948, https://doi.org/10.34194/geusb.v1.4695
Løseth, H., Rodrigues, N. and Cobbold, P.R. 2012. World's largest extrusive body of sand? *Geology*, **40**, 467–470, https://doi.org/10.1130/G33117.1
Løseth, H., Raulline, B. and Nygård, A. 2013. Late Cenozoic geological evolution of the northern North Sea: development of a Miocene unconformity reshaped by large-scale Pleistocene sand intrusion. *Journal of the Geological Society, London*, **170**, 133–145, https://doi.org/10.1144/jgs2011-165
Lowe, D.R. 1975. Water escape structures in coarse-grained sediments. *Sedimentology*, **22**, 157–204, https://doi.org/10.1111/j.1365-3091.1975.tb00290.x
MacLeod, M.K., Hanson, R.A., Bell, C.R. and McHugo, S. 1999. The Alba field ocean bottom cable seismic survey: impact on development. *Leading Edge*, **18**, 1306–1312, https://doi.org/10.1190/1.1438206
Marini, M., Della Porta, G., Felletti, F., Grasso, B.M., Franzini, M. and Casella, V. 2019. Insight into heterogeneous calcite cementation of turbidite channel-fills from UAV photogrammetry. *Geosciences*, **9**, 236, https://doi.org/10.3390/geosciences9050236
Matthews, K.J., Maloney, K.T., Zahirovic, S., Williams, S.E., Seton, M. and Müller, R.D. 2016. Global plate boundary evolution and kinematics since the late Paleozoic. *Global and Planetary Change*, **146**, 226–250, https://doi.org/10.1016/j.gloplacha.2016.10.002
McClay, K.R., Norton, M.G., Coney, P. and Davis, G.H. 1986. Collapse of the Caledonian orogen and the Old Red Sandstone. *Nature*, **323**, 147–149, https://doi.org/10.1038/323147a0
Müller, R.D., Cannon, J., *et al.* 2018. GPlates: Building a virtual Earth through deep time. *Geochemistry, Geophysics, Geosystems*, **19**, 2243–2261, https://doi.org/10.1029/2018GC007584
Olivarius, M., Weibel, R., Schovsbo, N.H., Olsen, D. and Kjøller, C. 2018. Diagenesis of Upper Jurassic sandstones of the Blokelv-1 core in the Jameson Land Basin, East Greenland. *GEUS Bulletin*, **42**, 65–84, https://doi.org/10.34194/geusb.v42.4310
Parize, O. and Friès, G. 2003. The Vocontian clastic dykes and sills: a geometric model. *Geological Society, London, Special Publications*, **216**, 51–72, https://doi.org/10.1144/GSL.SP.2003.216.01.05
Parize, O., Beaudoin, B. *et al.* 2007. A methodological approach to clastic injectites: from field analysis to seismic modeling – examples of the Vocontian Aptian and Albian injectites (southeast France). *AAPG, Memoirs*, **87**, 173–183, https://doi.org/10.1306/1209861M873262
Parsons, A.J., Whitham, A.G. *et al.* 2017. Structural evolution and basin architecture of the Traill Ø region, NE Greenland: a record of polyphase rifting of the East Greenland continental margin. *Geosphere*, **13**, 733–770, https://doi.org/10.1130/GES01382.1
Rundberg, Y. and Eidvin, T. 2015. Discussion on 'Late Cenozoic geological evolution of the northern North Sea: development of a Miocene unconformity reshaped by large-scale Pleistocene sand intrusion', *Journal of the Geological Society,* 170, 133–145. *Journal of the Geological Society, London*, **173**, 384–393, https://doi.org/10.1144/jgs2014-023
Ryseth, A.E., Similox-Tohon, D. and Thieβen, O. 2025. Tromsø–Bjørnøya composite tectono-sedimentary element, Barents Sea. *Geological Society, London, Memoirs*, **57**, 520–543, https://doi.org/10.1144/M57-2018-19
Satur, N., Hurst, A., Bang, A., Skjærpe, I. and Muehlboeck, S.A. 2021. Characteristics of a wing-like sandstone intrusion, Volund Field. *Geological Society, London, Special Publications*, **493**, 151–166, https://doi.org/10.1144/SP493-2017-309
Seidler, L., Steel, R., Stemmerik, L. and Surlyk, F. 2004. North Atlantic marine rifting in the Early Triassic: new evidence from East Greenland. *Journal of the Geological Society, London*, **161**, 583–592, https://doi.org/10.1144/0016-764903-063
SLB, 2022. Petrel (version 2022.9.1), https://www.slb.com/products-and-services/delivering-digital-at-scale/software/petrel-subsurface-software/petrel
Shoulders, S.J. and Cartwright, J. 2004. Constraining the depth and timing of large-scale conical sandstone intrusions. *Geology*, **32**, 661–664, https://doi.org/10.1130/G20654.1
Sollid, K., Henriksen, L.B., Hansen, J.O., Thieβen, O., Ryseth, A., Knight, S. and Groth, A. 2021. Johan Castberg: the first giant oil discovery in the Barents Sea. *AAPG, Memoirs*, **125**, 213–248, https://doi.org/10.1306/13742360MGF.8.3876
Steventon, M.J., Jackson, C.A.L. *et al.* 2021. Evolution of a sand-rich submarine channel–lobe system, and the impact of mass-transport and transitional-flow deposits on reservoir heterogeneity: Magnus Field, Northern North Sea. *Petroleum Geoscience*, **27**, 2020–2095, https://doi.org/10.1144/petgeo2020-095
Surlyk, F. 1987. Slope and deep shelf gully sandstones, Upper Jurassic, East Greenland. *AAPG Bulletin*, **71**, 464–475, https://doi.org/10.1306/94886ECF-1704-11D7-8645000102C1865D
Surlyk, F. 1990. Timing, style and sedimentary evolution of Late Palaeozoic–Mesozoic extensional basins of East Greenland. *Geological Society, London, Special Publications*, **55**, 107–125, https://doi.org/10.1144/GSL.SP.1990.055.01.05
Surlyk, F. 2003. The Jurassic of East Greenland: a sedimentary record of thermal subsidence, onset and culmination of rifting. *GEUS Bulletin*, **1**, 657, https://doi.org/10.34194/geusb.v1.4674
Surlyk, F. and Larsen, M. 2023. Coarse-grained, marine, sub-wave base, high-angle clinoform sets: a little-known outcrop facies illustrated by Jurassic examples from East Greenland. *Basin Research*, **35**, 1509–1529, https://doi.org/10.1111/bre.12763
Surlyk, F. and Noe-Nygaard, N. 2001. Sand remobilisation and intrusion in the upper Jurassic Hareelv formation of East Greenland. *Bulletin of the Geological Society of Denmark*, **48**, 169–188, https://doi.org/10.37570/bgsd-2001-48-10
Surlyk, F. and Noe-Nygaard, N. 2003. A giant sand injection complex: the Upper Jurassic Hareelv Formation of East Greenland. *Geologia Croatica*, **56**, 69–81, https://doi.org/10.4154/GC.2003.04
Surlyk, F., Callomon, J.H., Bromley, R.G. and Birkelund, T. 1973. Stratigraphy of the Jurassic–Lower Cretaceous sediments of Jameson Land and Scoresby Land, East Greenland. *Meddelelser om Grønland*, **193**, 1–95, https://doi.org/10.7146/mog.v193.149647
Surlyk, F., Gjelberg, J. and Noe-Nygaard, N. 2007. The Upper Jurassic Hareelv Formation of East Greenland: a giant sedimentary injection complex. *AAPG, Memoirs*, **87**, 141–149, https://doi.org/10.1306/1209858M871101
Surlyk, F., Alsen, P. *et al.* 2021. Jurassic stratigraphy of East Greenland. *GEUS Bulletin*, **46**, 1–122, https://doi.org/10.34194/geusb.v46.6521
Tillmans, F., Gawthorpe, R.L., Jackson, C.A.L. and Rotevatn, A. 2021. Syn-rift sediment gravity flow deposition on a Late Jurassic fault-terraced slope, northern North Sea. *Basin Research*, **33**, 1844–1879, https://doi.org/10.1111/bre.12538
Tingay, M.R., Hillis, R.R., Swarbrick, R.E., Morley, C.K. and Damit, A.R. 2007. 'Vertically transferred' overpressures in Brunei: evidence for a new mechanism for the formation of high-magnitude overpressure. *Geology*, **35**, 1023–1026, https://doi.org/10.1130/G23906A.1
Tripathy, G.R., Hannah, J.L. and Stein, H.J. 2018. Refining the Jurassic–Cretaceous boundary: Re–Os geochronology and depositional environment of Upper Jurassic shales from the Norwegian Sea. *Palaeogeography, Palaeoclimatology, Palaeoecology*, **503**, 13–25, https://doi.org/10.1016/j.palaeo.2018.05.005
Turner, C.C., Cronin, B.T. *et al.* 2018. The South Viking Graben: overview of Upper Jurassic rift geometry, biostratigraphy, and extent of Brae Play submarine fan systems. *AAPG, Memoirs*, **115**, 9–38, https://doi.org/10.1306/13652177M1153807
Underhill, J.R. and Partington, M.A. 1993. Use of genetic sequence stratigraphy in defining and determining a regional tectonic control on the Mid-Cimmerian Unconformity – implications for North Sea Basin development and the Global Sea Level Chart. *AAPG, Memoirs*, **58**, https://doi.org/10.1306/M58581C18
Vétel, W. and Cartwright, J. 2010. Emplacement mechanics of sandstone intrusions: insights from the Panoche Giant Injection Complex, California. *Basin Research*, **22**, 783–807, https://doi.org/10.1111/j.1365-2117.2009.00439.x
Vigorito, M. and Hurst, A. 2010. Regional sand injectite architecture as a record of pore-pressure evolution and sand redistribution in the shallow crust: insights from the Panoche Giant Injection Complex, California. *Journal of the Geological Society*, **167**, 889–904.
Vigorito, M., Hurst, A., Cartwright, J. and Scott, A. 2008. Regional-scale shallow crustal remobilization: processes and architecture. *Journal of the Geological Society, London*, **165**, 609–612, https://doi.org/10.1144/0016-76492007-096
Vigorito, M., Hurst, A., Scott, A.J., Stanzione, O. and Grippa, A. 2022. A giant sand injection complex: processes and implications for basin evolution and subsurface fluid flow. *American Journal of Science*, **322**, 729–794, https://doi.org/10.2475/06.2022.01
VRGeoscience Limited. 2022. Virtual reality Geological Studio (VRGS) (version 3.1), https://www.vrgeoscience.com
Waltham, R.J., Zvirtes, G., Burnham, B.S. and Hurst, A. 2025. Geometric and spatial analysis of wing-like intrusions as outcrop analogues for subsurface analysis. *Basin Research*, **37**, e70036, https://doi.org/10.1111/bre.70036
Zhang, Y. and Qu, Z. 2022. Distribution patterns of calcite cement in the turbidite sandstones of the Shahejie Formation in the Dongying Depression, Eastern China. *Acta Geologica Sinica-English Edition*, **96**, 1041–1056, https://doi.org/10.1111/1755-6724.14705
Zvirtes, G., Philipp, R.P., Hurst, A., Palladino, G., De Ros, L.F. and Grippa, A. 2020. Petrofacies of Eocene sand injectites of the Tumey Giant Injection complex, California (USA). *Sedimentary Geology*, **400**, 105617, https://doi.org/10.1016/j.sedgeo.2020.105617